The Thesis Committee for Hao Yao
certifies that this is the approved version of the following Thesis:

Coupling Viscous Vorticity Equation (VISVE) Method with OpenFOAM to Predict Turbulent Flow around 2-D Hydrofoils and Cylinders

Supervising Committee:

Spyros A. Kinnas, Supervisor

Kamy Sepehrnoori

Coupling Viscous Vorticity Equation (VISVE) Method with OpenFOAM to Predict Turbulent Flow around 2-D Hydrofoils and Cylinders

by

Hao Yao

THESIS

Presented to the Faculty of the Graduate School of

The University of Texas at Austin

in Partial Fulfillment

of the Requirements

for the Degree of

MASTER OF SCIENCE IN ENGINEERING

THE UNIVERSITY OF TEXAS AT AUSTIN

May 2019

Dedicated to my family for their support and love.

Acknowledgments

I would like to acknowledge the invaluable support from the following professors, colleagues, and friends. I appreciate the effort and time they have contributed to help me during my study at the Ocean Engineering Group (OEG) of the Department of Civil, Architectural and Environmental Engineering.

Firstly, I would like to express my deep gratitude to my supervisor Dr. Kinnas for his continuous support of my study and research, for his patience, motivation, and immense knowledge. His guidance helped me in all the time of research and writing of this thesis. I could not have imagined having a better supervisor for my master study.

I would also like to recognize my second reader, Dr. Kamy Sepehrnoori for his interest in my research. I appreciate him for all the deep thoughts and constructive comments. It is him who helped me complete a better master thesis.

In addition, I would like to express my sincere thanks to my colleagues at the Ocean Engineering Group (OEG), especially, former graduate students Dr. Ye Tian, Mr. Zhihao Li, Ms. Yunjun Wu and Ms. Lu Xing who laid the foundation for this work. I also wish to thank Mr. Chunlin Wu for his continuing efforts in improving VISVE and extending its abilities. I also

appreciate the help and suggestions Mr. Weikang Du and Dr. Yiran Su on the synchronous coupling work. I value the time spent with Mr. Seungnam Kim, who shared a lot of opinions on my study.

Finally, I am grateful to my parents Tao Yao and Jinhua Zhang for their utmost love and endless support through all my personal endeavors. Thank you for always being my Harbor of mind.

This work was partly by the US Office of Naval Research (Grant Number N00014-14-1- 0303 and N00014-18-1- 2276; Dr. Ki-Han Kim) by Phase VIII of the Consortium on Cavitation Performance of High Speed Propulsors.

Coupling Viscous Vorticity Equation (VISVE) Method with OpenFOAM to Predict Turbulent Flow around 2-D Hydrofoils and Cylinders

Hao Yao, M.S.E.
The University of Texas at Austin, 2019

Supervisor: Spyros A. Kinnas

The VIScous Vorticity Equation (VISVE) method has already been applied to solve the laminar flow around a cylinder and a hydrofoil at low Reynolds numbers. This method is more computationally efficient and spatially compact than a viscous flow method based on primitive variables. However, the VISVE method fails at high Reynolds numbers due to the effects of turbulence. In this thesis, a synchronous coupling method was developed to couple the VISVE and a turbulence model in OpenFOAM, enabling the VISVE method to solve the turbulent flow at high Reynolds numbers in a 2-D hydrofoil case and a 2-D cylinder case. The velocity, vorticity, and pressure calculated by the coupling method agree well with the results obtained by a RANS method.

Table of Contents

List of Tables

List of Figures

Nomenclature

This list describes several symbols that will be used within the body of the thesis

A_E^d	TDMA coefficient of the east side of the cell
A_P^d	TDMA coefficient of the center cell
A_W^d	TDMA coefficient of the west side of the cell
C_d	Drag coefficient, $C_d = \frac{F_{drag}}{\rho U_\infty^2 R}$
C_l	Lift coefficient, $C_l = \frac{F_{lift}}{\rho U_\infty^2 R}$
D	Diameter of cylinder
i	Indices in direction 1
j	Indices in direction 2
Q	TDMA coefficient on the right hand side of the TDMA equation
R	Radius of cylinder
Re	Reynolds number
T	Symmetric tensor of viscous stresses
U_∞	Unidirectional inflow velocity
$x_{(i,j)}$	X coordinate of cell centroid point (i, j)

$y_{(i,j)}$	Y coordinate of cell centroid point (i, j)
μ_m	Molecular viscosity, $\mu_m = \rho \cdot \nu_m$
μ_τ	Turbulent viscosity, $\mu_\tau = \rho \cdot \nu_\tau$
ν_m	Molecular kinematic viscosity
$\nu_{(i,j)}$	Turbulent viscosity of cell centroid point (i, j)
ν_τ	Turbulent kinematic viscosity
ω	Vorticity in vorticity equation

Chapter 1

Introduction

1.1 Background

Designing and accurately predicting the performance of propellers have been a challenge for naval engineers. The challenge involves not only the fulfillment of usual performance characteristics but also the optimization of performance in correspondence to very different operating conditions. Since the Boundary Element Method (BEM) cannot capture the leading-edge vortex, this method cannot predict the propellers' performance at very high loadings.

Due to this reason, the VIScous Vorticity Equation (VISVE) model[1] was developed to improve the prediction of off-design performance. The VISVE method was first implemented by Tian and Kinnas [9]. The VISVE model is able to calculating the complex flow separation, because this method solves the vorticity transport equation in the whole fluid field. The leading edge vortex predicted by VISVE and the RANS method is compared and shown in Figure 1.1.

[1]The main work of this thesis is based on Yao and Kinnas [17]. Even though the formulation of the turbulent vorticity equation was derived by Dr. Kinnas, the coupling of the VISVE method with OpenFOAM was implemented and tested by the author of this thesis.

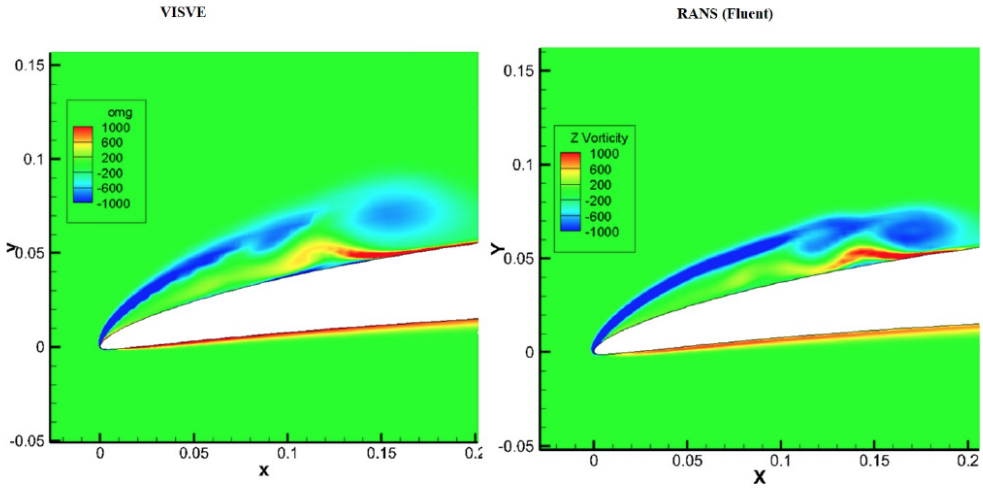

Figure 1.1: Leading edge vortex predicted by the VISVE and the RANS method from Tian [10].

The VISVE method was then applied in the case of 3-D hydrofoils in forwarding conditions as well as cylinders in unidirectional and alternating laminar flow by Wu [14], Li and Kinnas [7], and Wu *et al.* [13, 12]. Reliable results were obtained in all these applied cases. In short, the VIScous Vorticity Equation (VISVE) method could be applied to solve laminar flow around 2-D and 3-D hydrofoils as well as cylinders at low Reynolds numbers.

1.2 Motivation

The VISVE model has been well validated in laminar cases of 2-D hydrofoils and cylinders. However, problems arise as the VISVE method fails at high Reynolds numbers due to the effects of turbulence since the VISVE

method lacks the turbulent model to evaluate the turbulent viscosity. Therefore, an improvement in VISVE is needed.

In this paper, a synchronous coupling method was developed to couple the VISVE method with a turbulence model in OpenFOAM, an open source computational fluid dynamics (CFD) software. This synchronous coupling method was applied in 2-D hydrofoils and 2-D cylinders cases to predict turbulent flows at high Reynolds numbers. On one hand, VISVE has been found to be more computationally efficient and spatially compact than the RANS method, since it has a higher level of parallelization and a much smaller domain size. On the other hand, OpenFOAM is a good open source framework for users to build their own solvers by utilizing C++ libraries that have been already compiled within it. Hence, the coupling method is expected to be applied to solve turbulent flow with high computational efficiency.

1.3 Objectives

The objectives of this research are

- Conducting literature review of vortex methods as well as turbulence models.
- Describing two-dimensional VIScous Vorticity Equation (VISVE) method and recovering its results in the application to a 2-D hydrofoil case.
- Developing a synchronous coupling method to couple VISVE method with a turbulence model in OpenFOAM.

- Using the coupling method to enable the VISVE method to solve turbulent flows around 2-D hydrofoils and 2-D cylinders at high Reynolds numbers.

- Making conclusions and describing the future work.

1.4 Overview

This thesis consists of six chapters.

Chapter 1 contains background, motivation and objectives of this research.

Chapter 2 provides a brief literature review regarding vorticity methods, the developing history of VISVE and several turbulence models.

Chapter 3 presents the detailed mathematical formulations and numerical implementation of the coupling method. It also demonstrates the synchronous coupling scheme and the data transfer between the VISVE method and the turbulence model in OpenFOAM.

Chapter 4 consists of the applications to unidirectional inflow cases for 2-D hydrofoils and 2-D cylinders to predict turbulent flows at high Reynolds numbers. The predicted vorticity and velocity profiles, as well as the pressure coefficients are compared to those obtained from the RANS method.

The discussion of the results and the conclusions are included in Chapter 5 and Chapter 6.

Chapter 2

Literature Review

This chapter[1] reviews the related literature on two topics: vortex-based methods and turbulence models.

2.1 Vortex Method

2.1.1 History of Vortex Method

Vortex methods have been studied for a long time and applied to propeller flows extensively.

For airfoils, 2-D separated flow around them can be predicted by a discrete vortex method. Katz [4] used a discrete vortex method to analyze the separated unsteady inviscid flow around an airfoil. A 2-D airfoil under a high angle of attack was simulated using the vortex lattice approach and the periodic shedding vortex and forces were predicted in his work.

For propellers, Boundary Element Method (BEM) has been applied to analyze the unsteady flow around them. BEM was first introduced to solve 2-D flow around hydrofoils by Giesing [3] and then it was applied to propellers

[1]The main work of this thesis is based on Yao and Kinnas [17]. Even though the formulation of the turbulent vorticity equation was derived by Dr. Kinnas, the coupling of the VISVE method with OpenFOAM was implemented and tested by the author of this thesis.

by Kinnas and Hsin [6] who introduced an iterative pressure Kutta condition at the trailing edge of the blade.

The methods above all omit the effects of viscosity, which can be significant, especially at high-loading off-design conditions. Fortunately, the VIScous Vorticity Equation (VISVE) method makes up for the above shortcomings.

The VISVE method can capture the leading edge vortex which cannot be done by the two methods above. Tian and Kinnas [10] implemented the VISVE method firstly. This method has the advantages of needing a significantly smaller computational domain, higher computational efficiency, and automatically generated grids. Besides, the vorticity equation enjoys the absence of the pressure terms, which makes pressure evaluation not coupled with the vorticity transport equation. Due to these advantages, the method has been applied in the case of 2-D and 3-D hydrofoils, and 2-D cylinders in unidirectional and alternating flows by Wu [14], Li and Kinnas [7], and Wu *et al.* [13, 12]. In addition, Xing *et al.* [16] implemented a cavity mixture model in VISVE. As mentioned by Wu [13, 12], VISVE's efficiency can be improved significantly after parallelization. In contrast, the VISVE method needs fewer CPUs and spends much less computing time than the RANS method. Reliable results were obtained in all the applied cases.

2.1.2 Advantages of Vortex Method

The vortex method has three predominant advantages since it needs much smaller computational domains compared with the RANS method. This

is because that the vortex method describes the flow in terms of vorticity rather than velocity and pressure. Compared with velocity U, vorticity ω is a dimensionally compact variable, which means the volume of fluid with a significant amount of vorticity is typically of a relatively small fraction near the wall.

This feature of the VISVE method that requires a smaller computational domain contributes to its three advantages.

First of all, the VISVE method is more computational efficient than the RANS method.

Secondly, it can simplify the grid generating process. Actually, the computational grids can be generated automatically and the boundary conditions at far field can be automatically satisfied by using Green's function in VISVE.

Thirdly, the vorticity equation enjoys the absence of the pressure terms, which makes pressure evaluation decoupled with the vorticity transport equation. To be more specific, a simplified vorticity equation for incompressible, single-phase flow can be obtained by taking curl of the Navier-Stokes equation. The vorticity equation is shown as below:

$$\frac{\partial \omega}{\partial t} + \overrightarrow{q} \cdot \overrightarrow{\nabla} \omega = \omega \cdot \overrightarrow{\nabla} \overrightarrow{q} + \nu \nabla^2 \omega \tag{2.1}$$

where ω is the vorticity, $\overrightarrow{q}$ is the velocity, ν is the kinematic viscosity, t is the time. Thus, pressure evaluation is not needed when solving this vorticity

equation.

2.1.3 Disadvantages of Vortex Method

Despite all the advantages listed in the previous section, there are still some remaining challenges in using the vortex method. The biggest challenge is that the vorticity boundary condition on the foil or cylinder surface is implicit. This means that the researchers need to create vorticity at the boundary on the body surface to impose a torque onto the computational cells near the boundary.

In contrast, the interior boundary condition is straightforward in velocity-based method including the RANS method. In the RANS method, the researcher can either establish a Dirichlet boundary condition on velocity or a Neumann boundary condition on pressure, because both velocity and pressure are explicitly involved in Navier-Stokes equation.

Although many researchers endeavored to put forward methods to fix this difficulty, there is still no widely accepted mathematical convergence proof for these methods as described in Xing *et al.* [16].

2.2 Turbulence Model

However, the VISVE method would fail at high Reynolds numbers, as it needs to include the effects of turbulent-viscosity. As mentioned in Pope [8], turbulent-viscosity models are based on the turbulent-viscosity hypothesis which includes the intrinsic assumption and the gradient-diffusion hypothesis.

Turbulent models include algebraic models, one-equation models, and two-equation models.

2.2.1 k-ϵ Model

The k-epsilon (k-ϵ) turbulence model [8] is the most common two-equation model to simulate mean flow characteristics for turbulent flow conditions. The first transported variable is the turbulence kinetic energy (k) and the second transported variable is the rate of dissipation of turbulence energy (ϵ).

The k-ϵ model performs well specifically for planar shear layers and recirculating flows. However, it performs poorly in a variety of important cases such as unconfined flows, curved boundary layers, rotating flows and flows in non-circular ducts as mentioned in [8].

2.2.2 k-ω Model

The k-omega (k-ω) model is another two-equation model. The two essential variables used in this model are k and ω. k is the turbulence kinetic energy and ω is the specific rate of dissipation.

This model is superior both in its treatment of the viscous near-wall region and in its accounting for the effects of stream-wise pressure gradients.

2.2.3 k-ω (SST) Model

"SST" stands for Shear Stress Transport. The k-ω Shear Stress Transport (SST) model can solve the problem which k-ω model has in treating non-turbulent free-stream boundaries. Thus, I choose this model to be the turbulence model in OpenFOAM in this research.

Next chapter describes the methodology used in the VISVE method as well as the synchronous coupling method.

Chapter 3

Methodology

This chapter[1] consists of two parts, including the VIScous Vorticity Equation (VISVE) method and the synchronously coupling method.

3.1 The VISVE Method

Since the VIScous Vorticity Equation (VISVE) method is the basis of this thesis, this part revisited the VISVE method as described in Tian and Kinnas [10, 9].

3.1.1 Laminar Vorticity Equation

The laminar vorticity equation can be derived from the governing equation for incompressible viscous flow. The Navier-Stokes equations can be written as

$$\frac{\partial \overrightarrow{q}}{\partial t} + (\overrightarrow{q} \cdot \overrightarrow{\nabla})\overrightarrow{q} = -\frac{\overrightarrow{\nabla} p}{\rho} + \nu \nabla^2 q \tag{3.1}$$

[1]The main work of this thesis is based on Yao and Kinnas [17]. Even though the formulation of the turbulent vorticity equation was derived by Dr. Kinnas, the coupling of the VISVE method with OpenFOAM was implemented and tested by the author of this thesis.

In equation (3.1), $\overrightarrow{q}$ denotes the velocity vector, p and ρ represent the pressure and density, respectively, and ν is the kinematic viscosity. By simply taking the curl of this equation, we get the vorticity equation as given in Batchelor [2]:

$$\frac{\partial \overrightarrow{\omega}}{\partial t} + (\overrightarrow{q} \cdot \overrightarrow{\nabla})\overrightarrow{\omega} = (\overrightarrow{\omega} \cdot \overrightarrow{\nabla})\overrightarrow{q} + \nu \nabla^2 \overrightarrow{\omega} \tag{3.2}$$

In equation (3.2), $\overrightarrow{\omega}$ denotes the vorticity vector, defined as the curl of the velocity vector $\overrightarrow{q}$. In 2-D problems, the vortex stretching term vanishes. The vorticity vector ends up with a non-zero value in only one direction, perpendicular to the flow velocities. Thus, $\overrightarrow{\omega}$ is simplified as a scalar ω:

$$\frac{\partial \omega}{\partial t} + \overrightarrow{\nabla} \cdot (\omega \overrightarrow{q}) = \nu \nabla^2 \omega \tag{3.3}$$

In Tian's [10] work, the vorticity-velocity solver in 2-D can be implemented with the help of a stream function $\overrightarrow{\psi}$, which is defined as

$$\overrightarrow{\nabla} \times \overrightarrow{\psi} = \overrightarrow{q} \tag{3.4}$$

The vorticity $\overrightarrow{\omega}$ can be then defined in a way as below:

$$\overrightarrow{\nabla} \times (\overrightarrow{\nabla} \times \overrightarrow{\psi}) = \overrightarrow{\omega} \tag{3.5}$$

Since the stream function $\overrightarrow{\psi}$ satisfies the continuity equation, which is

$$\overrightarrow{\nabla} \cdot \overrightarrow{\psi} = 0 \tag{3.6}$$

Equation (3.5) will become like this:

$$\nabla^2 \overrightarrow{\psi} = -\overrightarrow{\omega} \tag{3.7}$$

In 2-D, equation (3.7) becomes a scalar equation:

$$\nabla^2 \psi = -\omega \tag{3.8}$$

The main part of the VISVE method is to solve equation (3.3) and equation (3.8) .

3.1.2 Boundary Conditions

The boundary condition setting is important for solving equation (3.3) and the turbulent vorticity equation (3.17) in the next section.

3.1.2.1 Solid Boundary Conditions

As mentioned in Tian [10], the wall boundary condition is specified as a constant on the body surface, which is

$$\frac{\partial \psi}{\partial s} = \overrightarrow{q} \cdot \overrightarrow{n} = 0 \tag{3.9}$$

where $\overrightarrow{n}$ represents the normal direction on the wall.

However, these solid boundary conditions cannot be satisfied directly and a scheme described in Figure 3.1 is needed to enforce these boundary conditions. This is because that the velocities calculated from vorticity field at the beginning of each time step do not satisfy the no-slip boundary conditions on the wall. Thus, a vorticity creation scheme based on the Boundary Element Method (BEM) is designed to eliminate tangential and normal velocity denoted as $\overrightarrow{q_n}$, $\overrightarrow{q_s}$ on the wall. After assigning the newly created vorticity into cells in the first layer, the non-slip boundary condition will then be satisfied. More details are presented in Tian [10], Wu [12], and Li and Kinnas [7].

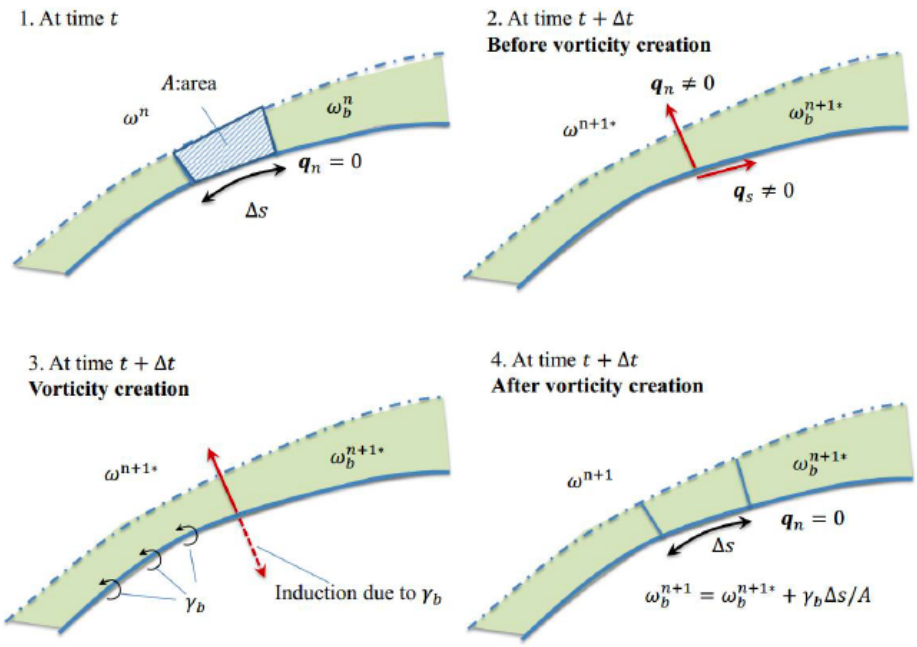

Figure 3.1: Schematic figure of the vorticity creation algorithm, from Tian [9].

3.1.2.2 Outer Boundary Conditions

The free space boundary conditions need to be consistent with the inflow velocity:

$$Inflow \begin{cases} \omega = 0 \\ U = U_\infty \end{cases} \tag{3.10}$$

$$Outflow \begin{cases} \frac{\partial \omega}{\partial n} = 0 \\ \frac{\partial U}{\partial n} = 0 \end{cases} \tag{3.11}$$

where $\overrightarrow{n}$ represents the normal direction of the outflow boundary. This means the vorticity is zero and the velocity equals the inflow velocity at the domain inflow free space boundary. In addition, a zero normal derivative condition is applied at the outflow free space boundary.

3.1.3 General Solving Algorithm

As mentioned in Tian [10] , and as summarized in Figure 3.2, the general solving strategy of the VISVE method has three components:

- Vorticity-velocity solver;
- VISVE solver;
- Vorticity creation.

The first step of solving the VISVE is to calculate the corresponding velocity field q of a given vorticity distribution. After obtaining q, the vorticity at the current time level ω^n will be marched to the next time level

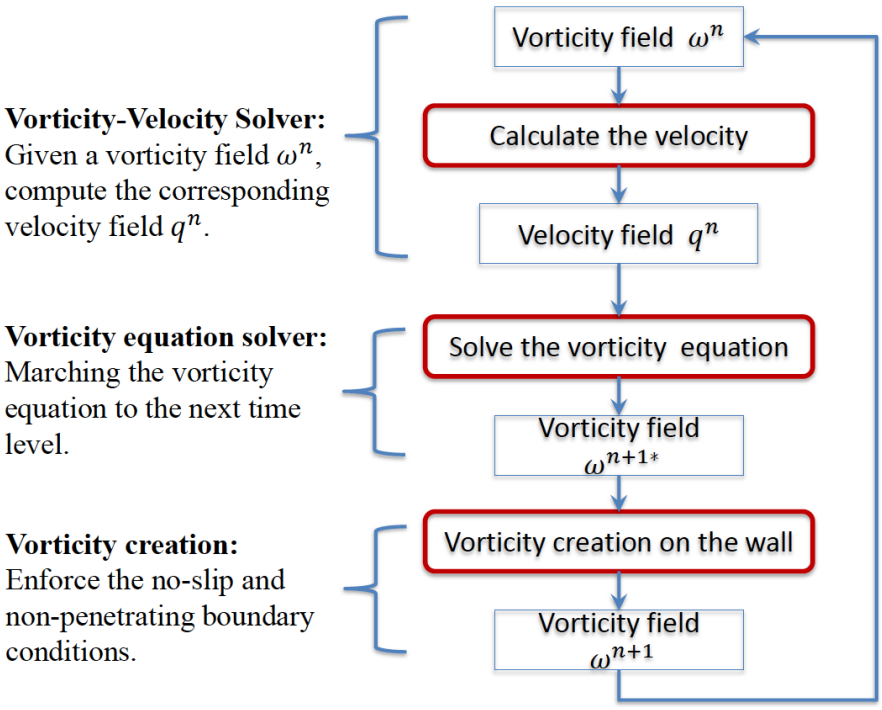

Figure 3.2: Flowchart of the solving procedures of VISVE in Tian [9].

$\omega^{n+1^\star}$. Because of the similarity between the VISVE and advection-diffusion equations, the former may be solved using the same techniques of solving the latter. However, $\omega^{n+1^\star}$ will not satisfy the boundary conditions on the wall. A correction on top of ω^{n+1} is necessary to represent the vorticity creation on the wall, in the meantime enforce the boundary conditions (both no-slip and non-penetrating). The correcting procedure is shown in Figure 3.1.

3.2 The Coupling Method

This part illustrated the coupling method, including the derivation of the turbulent vorticity equation, the numerical approach to solve the turbulent vorticity equation, and the general solving algorithm of the coupling scheme.

3.2.1 Turbulent Vorticity Equation

Based on the original VISVE model, the Vorticity Equation has been modified to include additional turbulent terms as described in Kinnas [5]. The turbulent vorticity equation is derived from the Navier-Stokes equation and is written down to the conservative form of turbulent vorticity equation. Considering the flow of a fluid, where $\overrightarrow{q} = (u_1, u_2, u_3)$ is the mean velocity in a x_1,x_2,and x_3 coordinate system, the Navier-Stokes equations are as follows:

$$\rho\frac{\partial\overrightarrow{q}}{\partial t} + \rho(\overrightarrow{q}\cdot\overrightarrow{\nabla})\overrightarrow{q} = -\overrightarrow{\nabla}p + \overrightarrow{\nabla}\cdot T - \overrightarrow{\nabla}\phi \tag{3.12}$$

where ρ is the density of the fluid, p is the mean pressure, ϕ is the potential of a conservative body force per unit volume, and T is the symmetric tensor of viscous stresses:

$$T = \begin{pmatrix} \tau_{11} & \tau_{12} & \tau_{13} \\ \tau_{21} & \tau_{22} & \tau_{23} \\ \tau_{31} & \tau_{32} & \tau_{33} \end{pmatrix} \tag{3.13}$$

with

$$\tau_{ij} = \mu[\frac{\partial u_i}{\partial x_j} + \frac{\partial u_j}{\partial x_i}] - \delta_{ij}\frac{2}{N}[\mu\overrightarrow{\nabla}\cdot\overrightarrow{q} + \rho k] \tag{3.14}$$

where $\mu = \mu_m + \mu_\tau$ is the total dynamic viscosity, with μ_m being the molecular viscosity and μ_τ being the turbulent viscosity of the fluid as described in Kinnas [5]. Taking the curl of both sides of equation (3.12), and using some vector identities, equation (3.12) will turn to a turbulent vorticity equation. For 2-D flow of fluid with constant density, the turbulent vorticity equation as described in Kinnas [5] is shown:

$$\begin{aligned}\frac{\partial \omega}{\partial t} + \overrightarrow{\nabla} \cdot (\omega \overrightarrow{q}) = \nabla^2((\nu_m + \nu_\tau)\omega) + 2\frac{\partial^2(\nu_m + \nu_\tau)}{\partial z^2}\frac{\partial \omega}{\partial x} \\ - 2\frac{\partial^2(\nu_m + \nu_\tau)}{\partial x^2}\frac{\partial u}{\partial z} + 4\frac{\partial^2(\nu_m + \nu_\tau)}{\partial x \partial z}\frac{\partial u}{\partial x}\end{aligned} \tag{3.15}$$

According to hydrofoil assumption, which is that $\frac{\partial}{\partial z} \gg \frac{\partial}{\partial x}$ especially within the narrow region close to the hydrofoil and its wake, the last three additional terms in equation (3.15) can be ignored. This makes:

$$\begin{aligned} 2\tfrac{\partial^2(\nu_m+\nu_\tau)}{\partial z^2}\tfrac{\partial \omega}{\partial x} &\approx 0 \\ -2\tfrac{\partial^2(\nu_m+\nu_\tau)}{\partial x^2}\tfrac{\partial u}{\partial z} &\approx 0 \\ 4\tfrac{\partial^2(\nu_m+\nu_\tau)}{\partial x \partial z}\tfrac{\partial u}{\partial x} &\approx 0 \end{aligned} \tag{3.16}$$

Thus, the vorticity equation for turbulent flow around a 2-D hydrofoil as describe in Kinnas [5] can be simplified to equation (3.17) below:

$$\frac{\partial \omega}{\partial t} + \overrightarrow{\nabla} \cdot (\omega \overrightarrow{q}) = \nabla^2((\nu_m + \nu_\tau)\omega) \tag{3.17}$$

3.2.2 Boundary Conditions

Equation (3.17) and equation (3.3) have the same wall boundary conditions and free space boundary conditions for velocity U and vorticity ω. In addition, the turbulent kinematic viscosity v_τ is zero on the wall and on the free space in equation (3.17), which is verified in the simulation result shown in Figure 4.14.

3.2.2.1 Solid Boundary Conditions

The wall boundary conditions for equation (3.17) are

$$\begin{cases} \frac{\partial \psi}{\partial s} = \overrightarrow{q} \cdot \overrightarrow{n} = 0 \\ \nu_\tau = 0 \end{cases} \tag{3.18}$$

Same as described in the previous subsection and Figure 3.1 , a vorticity creation scheme based on the Boundary Element Method (BEM) is designed to eliminate tangential and normal velocity denoted as $\overrightarrow{q_n}$, $\overrightarrow{q_s}$ on the wall. After assigning the newly created vorticity into cells in the first layer, the non-slip boundary condition will then be satisfied.

3.2.2.2 Outer Boundary Conditions

The free space boundary conditions for equation (3.17) are

$$Inflow \begin{cases} \omega = 0 \\ U = U_\infty \\ \nu_\tau = 0 \end{cases} \tag{3.19}$$

$$Outflow \begin{cases} \frac{\partial \omega}{\partial n} = 0 \\ \frac{\partial U}{\partial n} = 0 \\ \frac{\partial \nu_\tau}{\partial n} = 0 \end{cases} \tag{3.20}$$

where n represents the normal direction of the outflow boundary. Even with this boundary condition, the computational domain should still be built to be large enough to cover the vorticity field and make ν_τ to be zero at the outer boundary in order to obtain a converged solution for the coupling method.

3.2.3 Numerical Approach

The equation (3.17) is discretized in space by finite volume method:

$$\int_V \frac{\partial \omega}{\partial t} dV + \sum_{j=1}^{N} (\omega \overrightarrow{q} \overrightarrow{n} A)_j = \sum_{j=1}^{N} (\frac{\partial((\nu_m + \nu_\tau)\omega)}{\partial n_j} A)_j \tag{3.21}$$

The three terms are the unsteady term, convective term, and diffusive term. Equation (3.21) can be discretized into the numerical equation and the diffusive term can be treated based on the ADI scheme and TDMA method.

Let $\nu = \nu_m + \nu_\tau$, then equation (3.21) can be written into this form

$$\frac{\partial \omega}{\partial t} = -\frac{\partial U\omega}{\partial x} + \frac{\partial}{\partial x}(\frac{\partial(\nu\omega)}{\partial x}) - \frac{\partial V\omega}{\partial y} + \frac{\partial}{\partial y}(\frac{\partial(\nu\omega)}{\partial y}) \tag{3.22}$$

Let $H\omega = -\frac{\partial U\omega}{\partial x} + \frac{\partial}{\partial x}(\frac{\partial(\nu\omega)}{\partial x})$, $V\omega = -\frac{\partial V\omega}{\partial y} + \frac{\partial}{\partial y}(\frac{\partial(\nu\omega)}{\partial y})$, and apply the ADI scheme to equation (3.22). It can be separated into two equations below:

$$(1-\frac{\Delta tH}{2})\omega^{\star}=(1+\frac{\Delta tV}{2})\omega^{n} \tag{3.23}$$

$$(1-\frac{\Delta tV}{2})\omega^{n+1}=(1+\frac{\Delta tH}{2})\omega^{\star} \tag{3.24}$$

where ω^n is the vorticity at time step n and ω^{n+1} is the vorticity at time step n+1. Equation (3.23) can be solved by TDMA in x-direction and equation (3.24) can be solved by TDMA in the y-direction. Then integrate equation (3.23) and equation (3.24) over the cell volume and apply Gauss Theorem to get the numerical equation based on FVM. Finally, equation (3.23) and equation (3.24) can be solved in FVM form by TDMA. Focus on the term $\frac{\partial}{\partial y}(\frac{\partial(\nu\omega)}{\partial y})$.

$$\begin{aligned}\int \frac{\partial}{\partial y}(\frac{\partial(\nu\omega)}{\partial y})_i dV &= -\sum_f \frac{\partial(\nu\omega)}{\partial y}\Delta x\Omega_{cell} \\ &= [-\frac{\nu_{i+1}\omega_{i+1}-\nu_i\omega_i}{y_{i+1}-y_i}+\frac{\nu_i\omega_i-\nu_{i-1}\omega_{i-1}}{y_i-y_{i-1}}]\Delta x\Omega_{cell}\end{aligned} \tag{3.25}$$

The coordinates are described in Figure 3.3:

Equation (3.25) can be solved by TDMA method as shown in equation (3.26):

$$A_W^d\omega_{i-1}+A_P^d\omega_i+A_E^d\omega_{i+1}=Q \tag{3.26}$$

Compare equation (3.25) with equation (3.26):

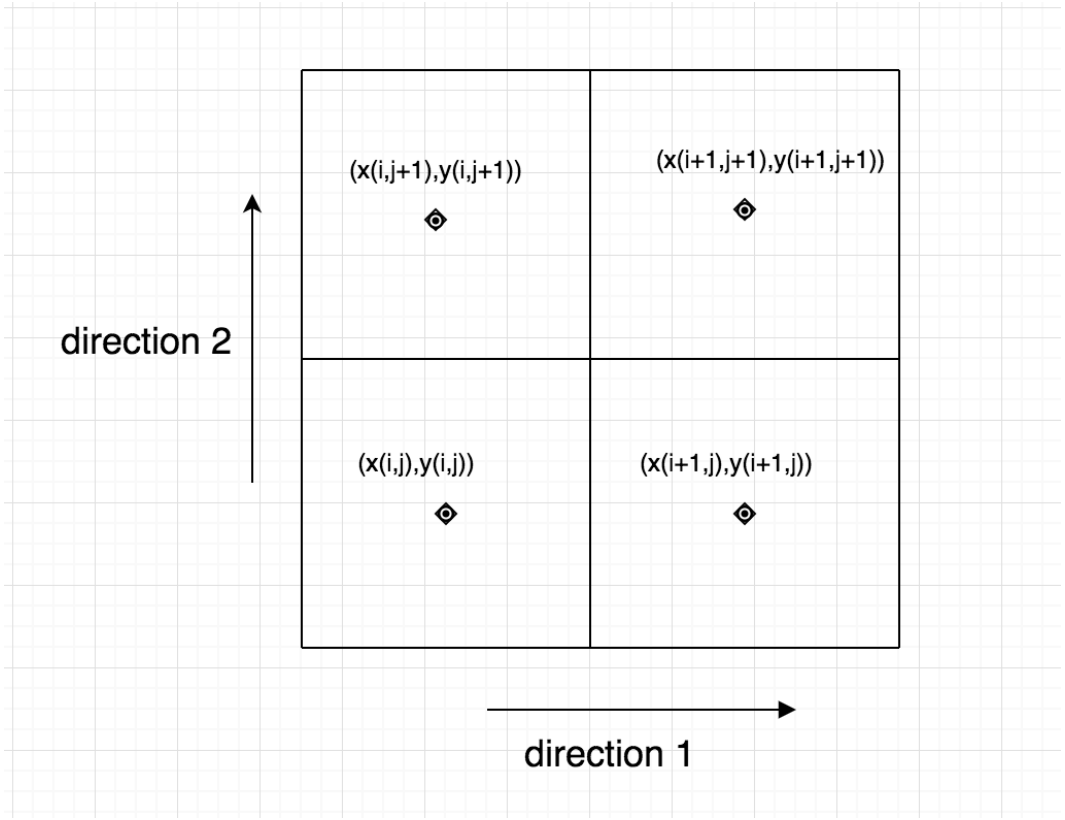

Figure 3.3: Coordinates for TDMA method.

$$\begin{aligned} A_W^d &= -\frac{\nu_{i-1}}{y_i - y_{i-1}} \Delta x \Omega_{cell} \\ A_P^d &= (\frac{\nu_i}{y_i - y_{i-1}} + \frac{\nu_i}{y_{i+1} - y_i}) \Delta x \Omega_{cell} \\ A_E^d &= -\frac{\nu_{i+1}}{y_{i+1} - y_i} \Delta x \Omega_{cell} \\ Q &= 0 \end{aligned} \tag{3.27}$$

The TDMA method can be conducted as following to solve ω. The TDMA coefficients for the diffusive term are shown in Table 3.1:

Table 3.1: TDMA coefficients for the diffusive term.

Equation	$\frac{\partial \omega}{\partial t} + \overrightarrow{\nabla} \cdot (\omega \overrightarrow{q}) = \nabla^2((\nu_m + \nu_\tau)\omega)$
Diffusive Flux in the 1^{st} Direction	$\frac{\omega_{(i+1,j)}\nu_{(i+1,j)} - \omega_{(i,j)}\nu_{(i,j)}}{x_{(i+1,j)} - x_{(i,j)}} \times (y_{n(i,j-1)} - y_{n(i,j)})$
A_W^d	$-\frac{\nu_{i-1}}{y_i - y_{i-1}} \Delta x \Omega_{cell}$
A_P^d	$(\frac{\nu_i}{y_i - y_{i-1}} + \frac{\nu_i}{y_{i+1} - y_i}) \Delta x \Omega_{cell}$
A_E^d	$-\frac{\nu_{i+1}}{y_{i+1} - y_i} \Delta x \Omega_{cell}$

$$
\begin{aligned}
A_P^{d_i} &= A_P^{d_i} + \frac{A_W^{d_i} A_E^{d_{i-1}}}{A_P^{d_{i-1}}} \qquad (i = 2, 3, \cdots, N) \\
Q_i^\star &= Q_i - \frac{A_W^{d_i} Q_{i-1}^\star}{A_P^{d_{i-1}}} \qquad (i = 2, 3, \cdots, N) \\
\omega_i &= \frac{Q_i^\star - A_E^{d_i} \omega_{i+1}}{A_P^{d_i}} \qquad (i = N, N-1, \cdots, 2)
\end{aligned}
\tag{3.28}
$$

The parameters in Table 3.1 are defined as below:

- i: Indices in direction 1;
- j: Indices in direction 2;
- $x_{(i,j)}$: x coordinate of Cell Centroid Point (i, j);
- $y_{(i,j)}$: y coordinate of Cell Centroid Point (i, j);
- $\nu_{(i,j)}$: turbulent viscosity of Cell Centroid Point (i, j);

The boundary conditions for equation (3.17) are described in equations (3.18) to equation (3.20).

3.2.4 Turbulence Model

The k-Omega Shear Stress Transport (SST) model was utilized in both OpenFOAM and ANSYS Fluent because it can treat the viscous near-wall

region and non-turbulent free-stream boundaries very well as described in the previous section. The two essential variables used in this model are k and ω. k is the turbulence kinetic energy and ω is the specific rate of dissipation which is defined as

$$\omega = \frac{\epsilon}{k} \tag{3.29}$$

where ϵ is the rate of dissipation of turbulence energy. As described in Pope [8], the model equation for k-Omega SST model is

$$\frac{\partial \omega}{\partial t} + < U_i > \frac{\partial \omega}{\partial x_i} = \nabla \cdot (\frac{\nu_T}{\sigma_\omega} \nabla \omega) + C_{\omega 1} \frac{P\omega}{k} - C_{\omega 2} \omega^2 \tag{3.30}$$

where $< U_i >$ is the mean velocity in i^{th} direction, P is the production of turbulence kinetic energy (TKE), ν_T is the turbulent kinematic viscosity, $C_{\omega 1}$ and $C_{\omega 2}$ are the parameters where $C_{\omega 1} = 0.44$ and $C_{\omega 2} = 0.92$.

3.2.5 General Solving Algorithm

The coupling work is done iteratively. Within each iteration step, the turbulent viscosity ν_τ obtained from the turbulence model in OpenFOAM is imported into VISVE to solve the turbulent vorticity equation and get the velocity field U and V. The velocity information obtained from VISVE is then passed back into OpenFOAM to calculate the turbulent viscosity ν_τ in the next iteration step. The methodology is shown in Figure 3.4:

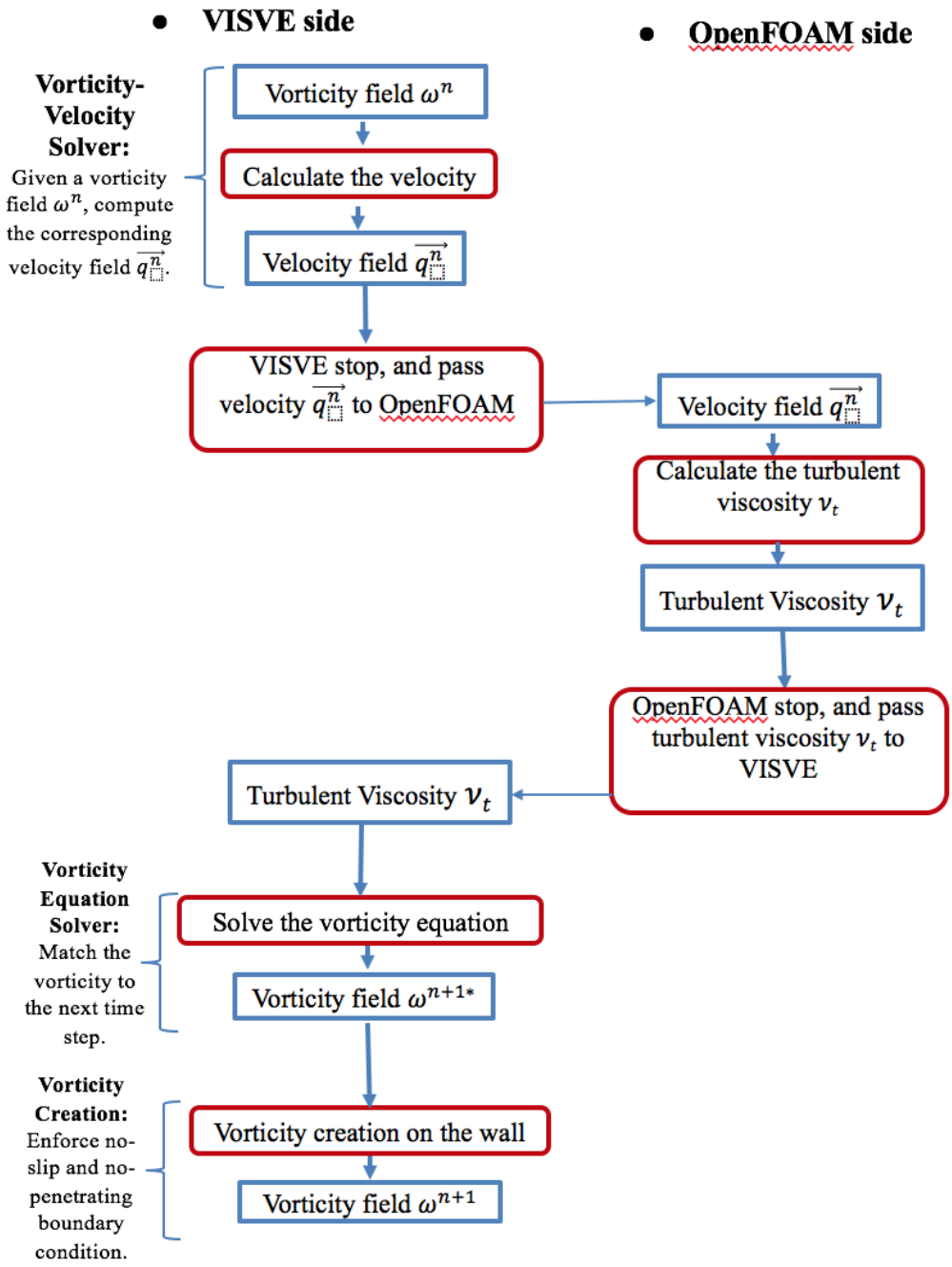

Figure 3.4: Flowchart of the solving procedures of the coupling method.

3.2.6 Pressure and Force Calculation

As mentioned in Li and Kinnas [7], unlike the RANS method, the VISVE method solves for velocity and vorticity. Thus, pressure around the body surface and forces can be obtained by post-processing.

3.2.6.1 Pressure Calculation for Hydrofoil Cases

In this thesis, the pressure on hydrofoil surface is obtained by doing integration from point B on the outer boundary to point A on the surface of the hydrofoil, as described in Li and Kinnas [7]

The total head H is defined as below:

$$H = \frac{\overrightarrow{q}^2}{2} + \frac{P}{2} \tag{3.31}$$

The gradient of the total head can be obtained from the N-S equation, as follows:

$$\overrightarrow{\nabla} H = -\frac{\partial \overrightarrow{q}}{\partial t} + \overrightarrow{q} \times \overrightarrow{\omega} - \nu_m \overrightarrow{\nabla} \times \overrightarrow{\omega} \tag{3.32}$$

Only the molecular kinematic viscosity ν_m is included in equation (3.32). After integration from point B on the outer boundary to point A on the surface of the hydrofoil, the pressure on the hydrofoil surface P_A can be obtained:

$$P_B = P_A + \rho(\int_A^B \overrightarrow{\nabla} H ds + \frac{\overrightarrow{q_A}^2 - \overrightarrow{q_B}^2}{2}) \tag{3.33}$$

3.2.6.2 Pressure Calculation for Cylinder Cases

In this thesis, the pressure on cylinder surface is obtained by doing integration along cylinder surface, which is described in Li and Kinnas [7]

The unsteady term $\frac{\partial q}{\partial t}$ and the convection term $(q \cdot \nabla)q$ vanish on the wall because of the no-slip boundary condition. After introducing a local coordinate system θ-r on the cylinder surface as shown in Figure 3.5, a relationship between pressure and vorticity can be obtained:

$$\frac{\partial P_0}{\partial \theta} = -\frac{\partial(\mu_m \omega_0)}{\partial r} \tag{3.34}$$

Only the molecular viscosity μ_m is included in equation (3.34) where P_0 and ω_0 represent pressure and vorticity on the cylinder, θ indicates the tangential direction and r is the normal direction.

Assuming that the stagnation point stays at the leading edge of the cylinder, the surface pressure along the wall boundary can be determined through integration by using the Bernoulli Equation. The surface pressure is shown in equation (3.35):

$$P_0(\theta) = \int_0^{2\pi} (-\frac{\partial(\mu_m \omega_0)}{\partial r}) d\theta + \frac{\rho U_\infty^2}{2} \tag{3.35}$$

The viscous shear stress would be needed in order to calculate the drag and lift force:

$$\tau = -\frac{\partial(\mu_m u_0)}{\partial r} = \mu_m \omega_0 \tag{3.36}$$

where u_0 is the velocity parallel to the cylinder surface and ω_0 is the vorticity. The drag and lift coefficient can be calculated as follows:

$$C_d = \frac{R\int_0^{2\pi}(R\frac{\partial(\mu_m\omega_0)}{\partial r}\cdot\mu_m\omega_0)sin\theta d\theta}{\rho U_\infty^2 R} \tag{3.37}$$

$$C_l = \frac{R\int_0^{2\pi}(R\frac{\partial(\mu_m\omega_0)}{\partial r}\cdot\mu_m\omega_0)cos\theta d\theta}{\rho U_\infty^2 R} \tag{3.38}$$

where R is the radius of the cylinder, U_∞ is the inflow velocity, ρ is the density of the fluid, and θ is the angle of a point on the cylinder as shown in Figure 3.5.

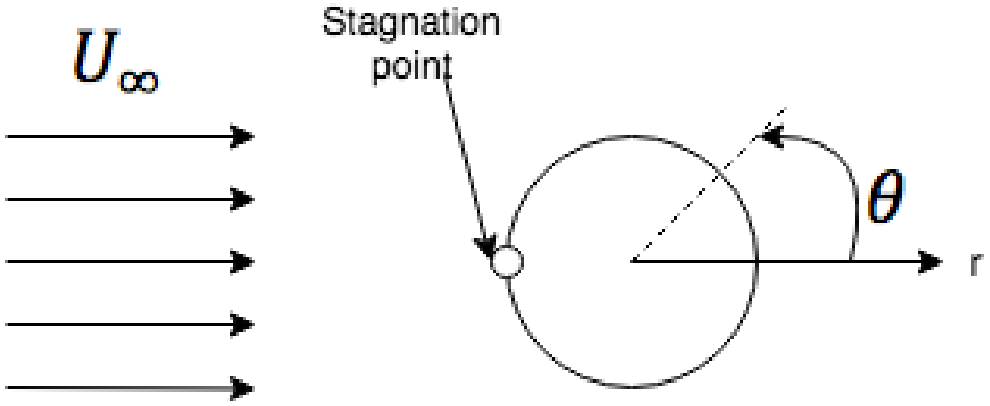

Figure 3.5: Local θ-r coordinate system on the cylinder surface.

Chapter 4

Applications to Hydrofoil and Cylinder Cases

This chapter[1] consists of two sections, including "laminar flow cases" and "turbulent flow cases".

4.1 Laminar Flow around a 2-D Hydrofoil Case

The goal of the first section is to recover the results calculated by Tian [10] in laminar flow around a 2-D hydrofoil case.

The VISVE method and the RANS method are applied in the case of 2-D hydrofoil at a 0-degree AOA. The hydrofoil is 4% thick (NACA 66) with 1% camber (NACA 0.8). The total chord length is 1 m. The velocity of the incoming flow is 2 m/s with an angle of attack to be 0 degree. The Reynolds number in the viscous case is specified to be 2×10^3 .

[1]The main work of this thesis is based on Yao and Kinnas [17]. Even though the formulation of the turbulent vorticity equation was derived by Dr. Kinnas, the coupling of the VISVE method with OpenFOAM was implemented and tested by the author of this thesis.

4.1.1 Grid Configuration

4.1.1.1 VISVE

As shown in the convergence study in the next sub-section, the domain parameters of Case #1 are good enough for the calculation to converge. Thus, we set the domain parameters to be the same as the ones in Case #1. The domain parameters and grids of VISVE method are shown in Table 4.1 and Figure 4.1.

Table 4.1: Domain parameters of VISVE method for laminar hydrofoil case, $\mathrm{Re} = 2 \times 10^3$.

	First Layer Height/ m	Expansion Ratio	Layer Number	Cell Number
Block 1	1×10^{-4}	1.095	45	17,415
Block 2	1×10^{-4}	1.05	60	5,400

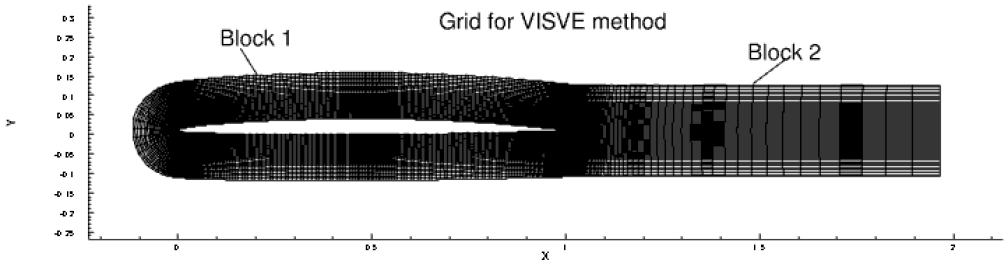

Figure 4.1: Grids of the VISVE method for laminar hydrofoil case, $\mathrm{Re} = 2 \times 10^3$.

4.1.1.2 RANS

In contrast, the domain parameters and grids of the RANS method are shown in Table 4.2 and Figure 4.2.

Table 4.2: Domain parameters of RANS method for laminar hydrofoil case, $Re = 2 \times 10^3$.

Cell Number	Number of Layer of Cells	First layer Height/ m	Expansion Ratio	Time Step Size/ s
150,000	80	3.5×10^{-4}	1.05	0.001

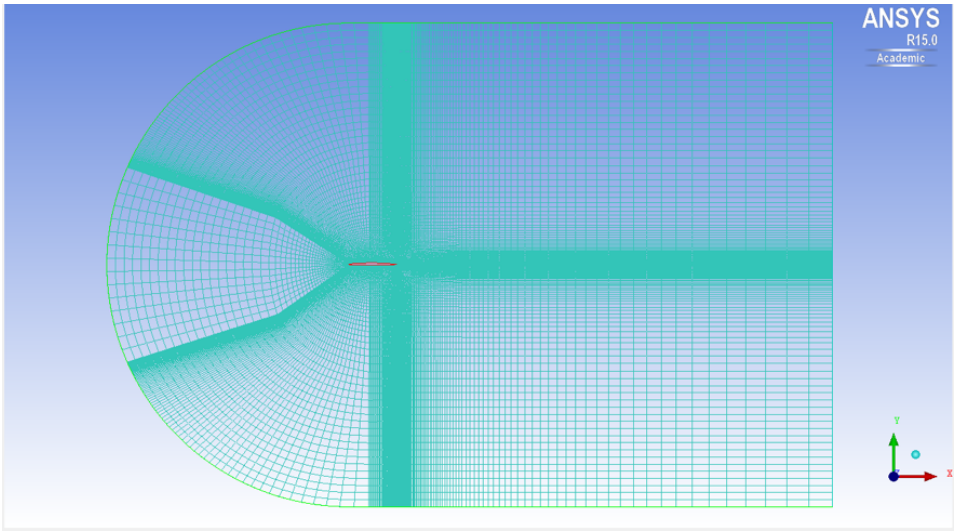

Figure 4.2: Grids of the RANS method for laminar hydrofoil case, $Re = 2 \times 10^3$.

The comparison of domains reveals that the RANS method needs to generate a structured mesh with good realization and needs a very large domain, which causes low computing efficiency.

This is due to two reasons. Firstly, the domain needs to be large enough to eliminate the effects of the boundary on the flow field. Secondly, the grids need to be fine enough to obtain a small first boundary layer height in laminar cases and a small dimensionless wall distance (y+) in turbulent cases.

In contrast, the VISVE method needs much fewer grids, making the run to be dimensionally compact and computationally efficient.

4.1.2 Comparison between two Methods

The computing comparison is made between the VISVE method and the RANS method in this laminar 2-D hydrofoil case. ANSYS Fluent (2019), a commercial CFD software is utilized to perform the RANS method.

The computation is performed at stampede2, the flagship supercomputer at the Texas Advanced Computing Center (TACC), the University of Texas at Austin. Currently, the VISVE method has been tested by using 1 CPU while the RANS method uses 48. The simulation time and CPU cost comparison is shown in Table 4.3.

Table 4.3: Simulation time and CPU cost comparison for laminar hydrofoil case, Re $= 2 \times 10^3$.

	VISVE	Fluent
Node Type	Intel Xeon Platinum 8160 ("Skylake")	Intel Xeon Platinum 8160 ("Skylake")
MPI: No. of CPUs	1	48
CPU Time	1 h 22 mins	1 h 45 mins
Time Step Size	$5 \times 10^{-4} s$	$5 \times 10^{-4} s$
Simulation Time	10 s	10 s

The velocity and vorticity comparison are shown from Figure 4.3 to Figure 4.8 below:

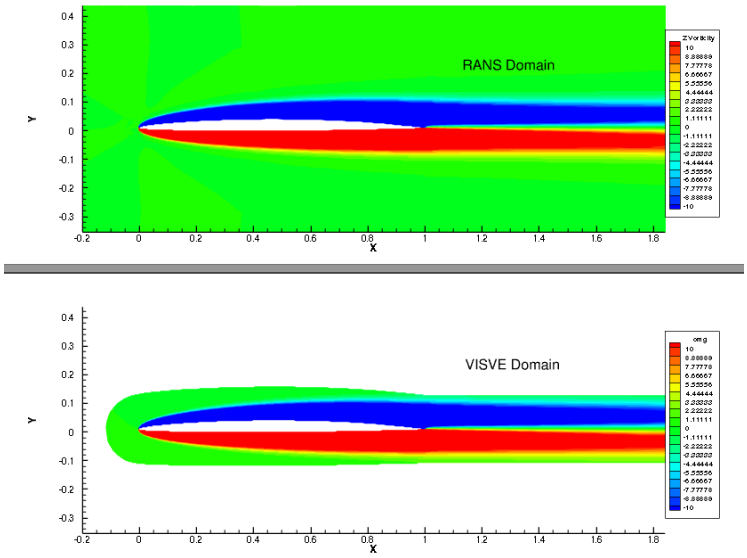

Figure 4.3: Vorticity contour at t =10 s, laminar flow, Re=2,000, hydrofoil case.

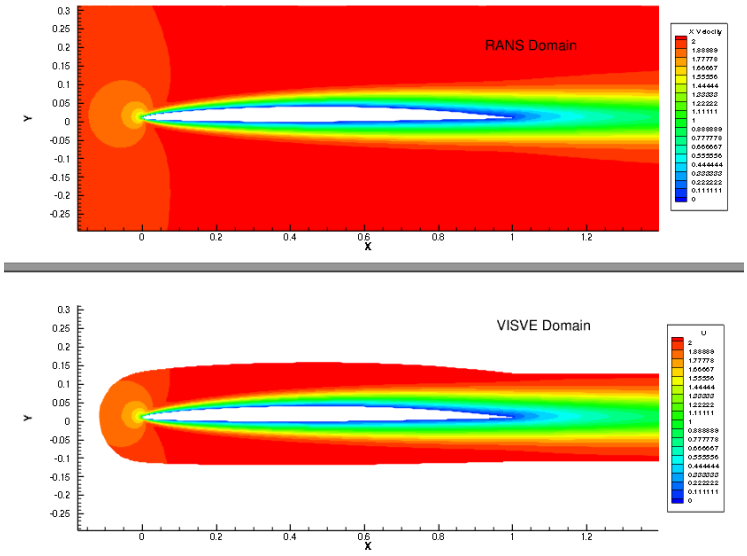

Figure 4.4: X-Velocity contour comparison at t =10 s, laminar flow, Re=2,000, hydrofoil case.

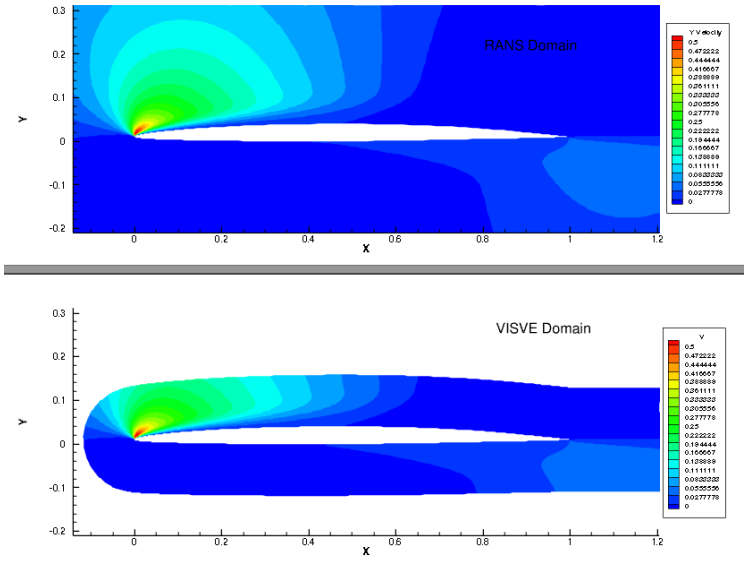

Figure 4.5: Y-Velocity contour comparison at t =10 s, laminar flow, Re=2,000, hydrofoil case.

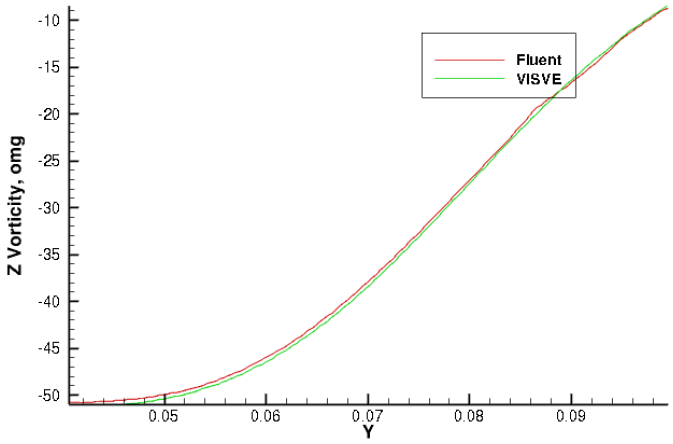

Figure 4.6: Vorticity profile comparison at hydrofoil midpoint at t =10 s, laminar flow, Re=2,000, hydrofoil case.

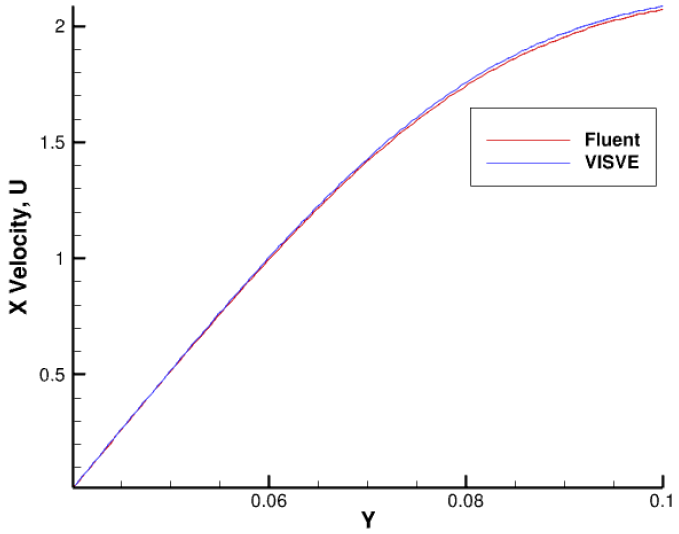

Figure 4.7: X-Velocity comparison at hydrofoil midpoint at t =10 s, laminar flow, Re=2,000, hydrofoil case.

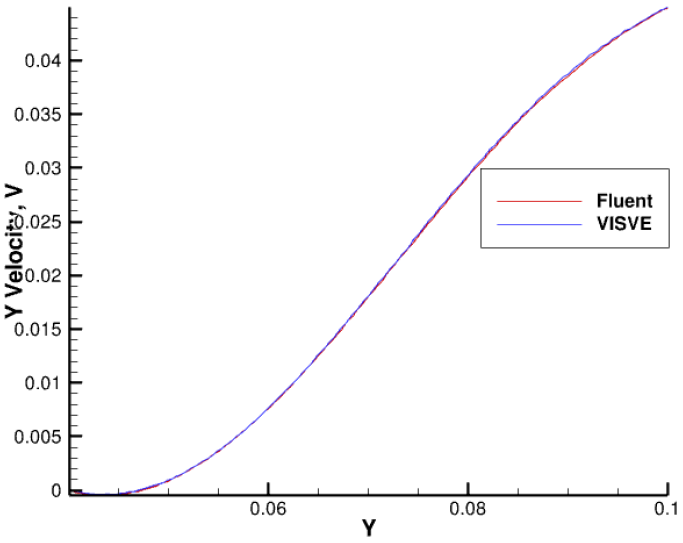

Figure 4.8: Y-Velocity comparison at hydrofoil midpoint at t =10 s, laminar flow, Re=2,000, hydrofoil case.

The pressure coefficients comparison between the VISVE method and the RANS method are shown in Figure 4.9.

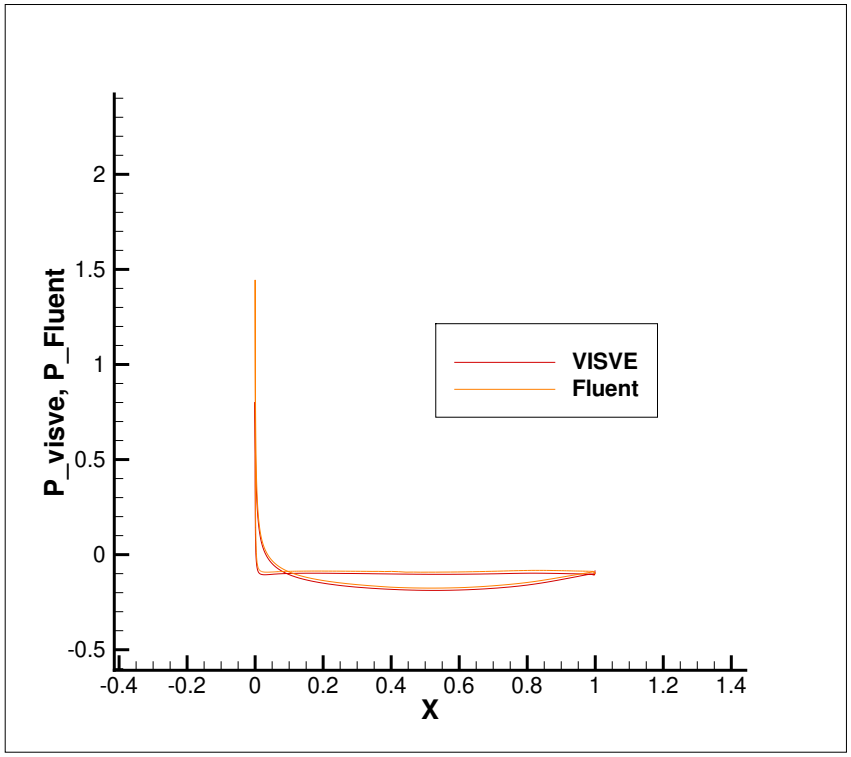

Figure 4.9: Pressure coefficients comparison at t =10 s, laminar flow, Re=2,000, hydrofoil case.

The VISVE results agree well with the RANS results. Even though the VISVE method utilizes only 1 CPU, it requires less CPU time than the RANS method, which requires 48 CPUs to get to the same simulation time.

4.1.3 Convergence Study

In order to validate the grid independence of the VISVE method, different sizes and different number of elements on the direction normal to the

hydrofoil surface have been applied to the 2-D VISVE model to predict the flow around the hydrofoil in laminar case. Three cases are designed as shown in Table 4.4. The tests are run at Re = 2,000, $AOA = 0^o$. The vorticity, x-velocity, and y-velocity at the half chord length from different cases agrees very well with each other as shown from Figure 4.10 to Figure 4.12, which validates the convergence of the VISVE model in the hydrofoil laminar case.

Table 4.4: Cases setting for grid independence study in laminar foil cases, $Re = 2 \times 10^3$.

Case No.	No. of Layers of Cell	First Layer Height/ m	Expansion Ratio in Block 1	No. of Elements on the Wake	Expansion Ratio in Block 2
1	45	1×10^{-4}	1.05	60	1.095
2	60	1×10^{-4}	1.05	70	1.095
3	75	1×10^{-4}	1.05	80	1.095

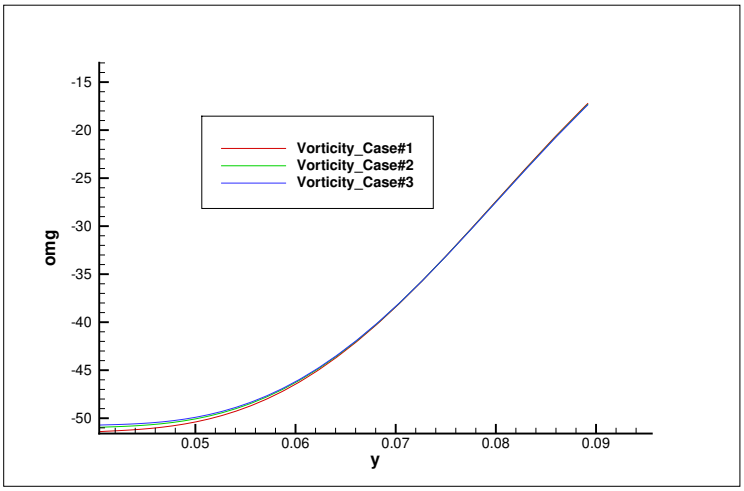

Figure 4.10: Comparison of vorticity at 50% chord length for different cases, Re=2,000, hydrofoil case.

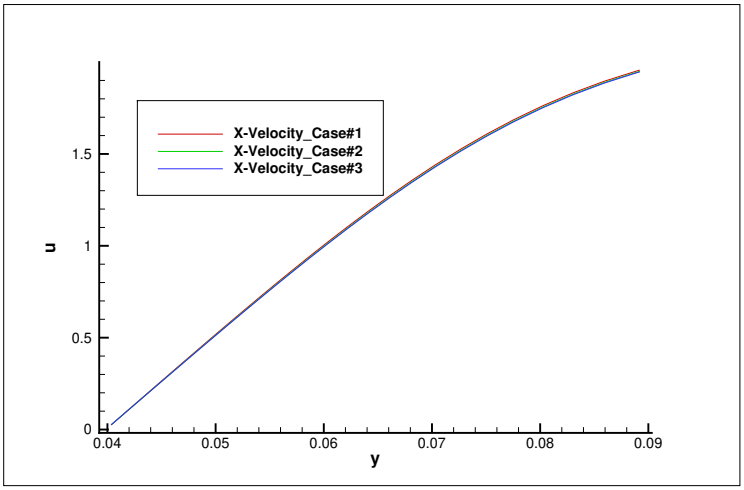

Figure 4.11: Comparison of X-velocity at 50% chord length for different cases, Re=2,000, hydrofoil case.

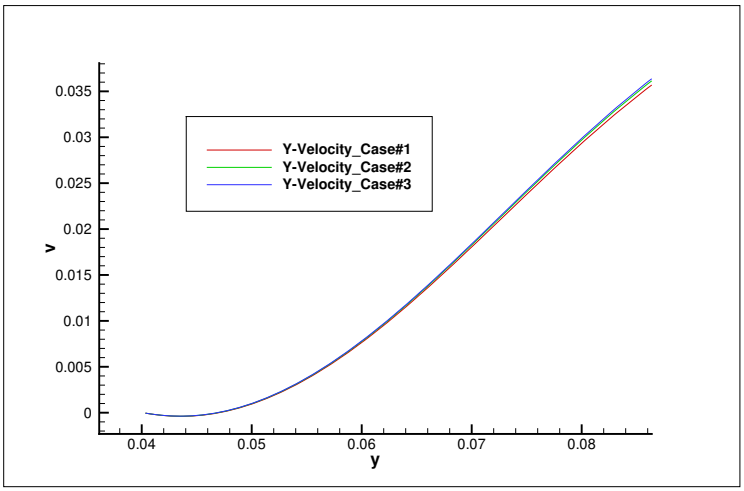

Figure 4.12: Comparison of Y-velocity at 50% chord length for different cases, Re=2,000, hydrofoil case.

4.2 Turbulent Cases

The coupling method is applied in a 2-D hydrofoil case and a 2-D cylinder case. Grid independence study is made and the results are compared with the RANS method. All RANS results shown in the next sections have been produced by using ANSYS-Fluent [1] and OpenFOAM.

4.2.1 Turbulent Flow around a Hydrofoil Case

The coupling method is applied in the case of 2D hydrofoil at a 0-degree AOA. The hydrofoil is 4% thick (NACA 66) with 1% camber (NACA 0.8). The total chord length is 1 m. Three different cases at three different Reynolds numbers were conducted within this section. The Reynolds numbers of these 3 cases are 10^6, 2×10^6, and 4×10^6, separately. The comparison is made between the coupling method and RANS method which is conducted by ANSYS Fluent [1] and OpenFOAM in the turbulent 2-D hydrofoil case.

For these 3 cases, the vorticity profiles and the velocity profiles between the coupling method and the RANS method are compared at location A, B, C, and D. Location A, B, C and D are shown in Figure 4.13:

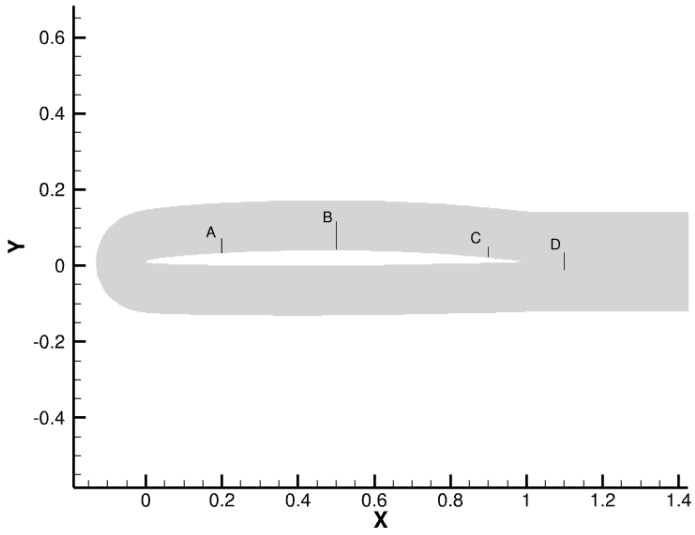

Figure 4.13: Demonstration for location A, B, C, and D.

For coupling case, the turbulent kinematic viscosity is narrowed in the small area that is close to the hydrofoil, which means the domain size does not influence the computational accuracy of turbulent viscosity result calculated by RANS method. To prove this, two RANS simulations with the large regular RANS domain and the small VISVE domain were conducted and the turbulent viscosities were compared in Figure 4.14 and Figure 4.15.

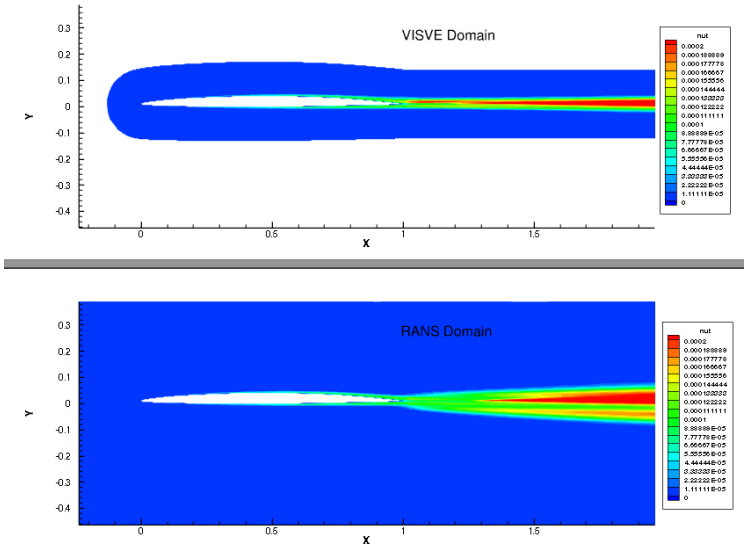

Figure 4.14: Turbulent viscosity contour comparison, turbulent flow, Re= 2×10^6 (above: OpenFOAM with VISVE domain; below: OpenFOAM with large RANS domain).

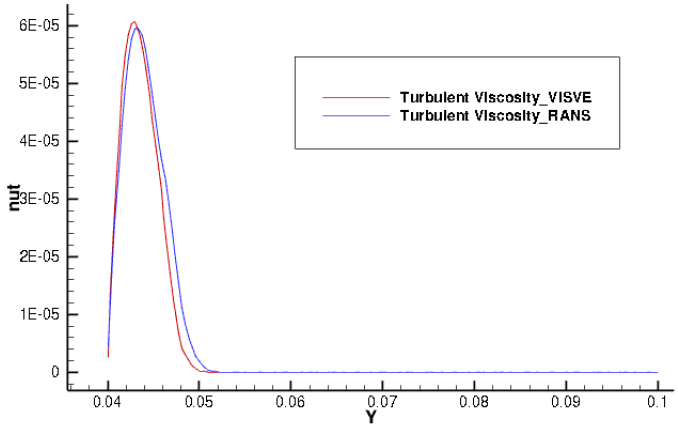

Figure 4.15: ν_τ profile comparison at x = 0.5 m, turbulent flow, Re= 2×10^6.

The turbulent viscosity calculated by OpenFOAM with the small VISVE

domain and the large RANS domain agrees well with each other. This proves that on the OpenFOAM side the small VISVE domain can be used instead of the large RANS domain in the coupling method.

4.2.1.1 Grid Configuration

After a grid independence study, the most appropriate domain for the coupling method with both good accuracy and the least computational time has been set.

The coupling method: As shown in the convergence study in the next subsection, the domain parameters of Case #1 are good enough for the calculation to converge. Thus, we set the domain parameters to be the same as the ones in Case #1. The domain parameters and grids of the coupling method are shown in Table 4.5 and Figure 4.16.

Table 4.5: Domain parameters of the coupling method for turbulent hydrofoil case, Re = 10^6, 2×10^6, and 4×10^6, separately.

	First Layer Height/ m	Expansion Ratio	Layer Number	Cell Number
Block 1	1×10^{-4}	1.095	50	19,350
Block 2	1×10^{-4}	1.05	85	8,500

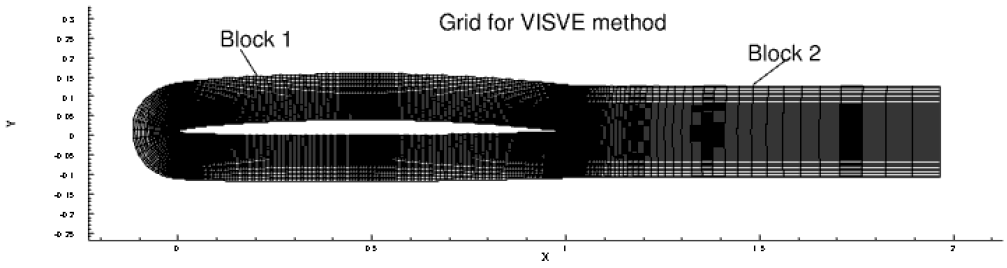

Figure 4.16: Grids of the the coupling method for turbulent hydrofoil case, $\mathrm{Re} = 10^6$, 2×10^6, and 4×10^6, separately.

RANS: In contrast, the domain parameters and grids of the RANS method are shown in Table 4.6 and Figure 4.17.

Table 4.6: Domain parameters of RANS method for turbulent hydrofoil case, $\mathrm{Re} = 10^6$, 2×10^6, and 4×10^6, separately.

Cell Number	Number of Layer of Cells	First Layer Height/ m	Expansion Ratio	Time Step Size/ s
150,000	80	3.5×10^{-4}	1.05	0.001

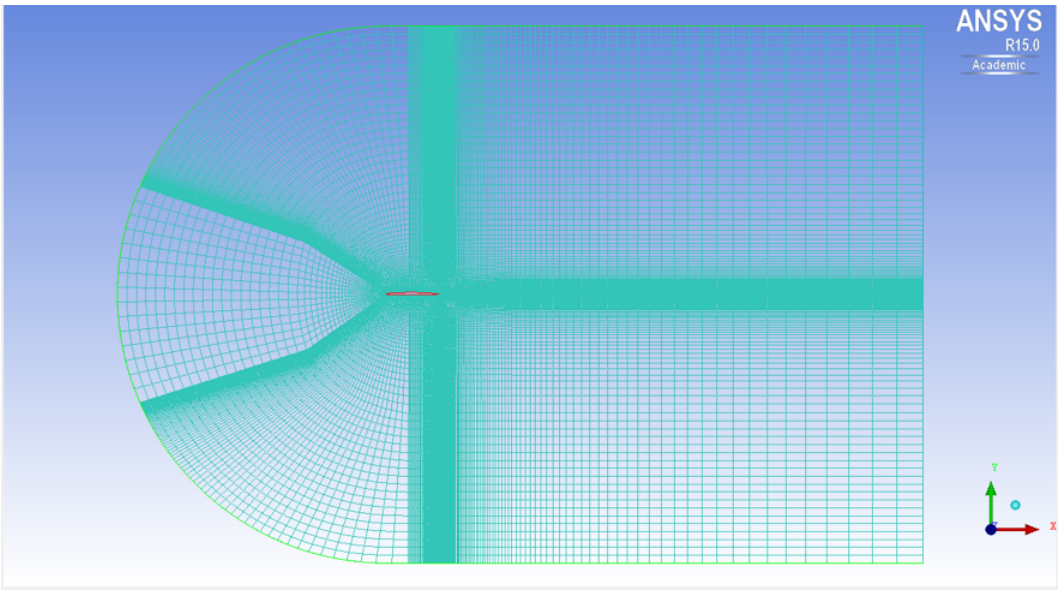

Figure 4.17: Grids of the RANS method for turbulent hydrofoil case, Re = 10^6, 2×10^6, and 4×10^6, separately.

4.2.1.2 Re = 2×10^6

The velocity of the incoming flow is 2 m/s with the angle of attack to be 0 degree. The Reynolds number in the viscous case is specified to be 2×10^6.

The simulation time and CPU cost comparison are shown in Table 4.7. The coupling method utilizes only 1 CPU and it requires only 2 times longer CPU time than the RANS method, which requires 48 CPUs to get to the same simulation time.

Table 4.7: Simulation time and CPU cost comparison for turbulent hydrofoil case, Re $= 2 \times 10^6$.

	Coupling Method	Fluent
Node Type	Intel Xeon Platinum 8160 ("Skylake")	Intel Xeon Platinum 8160 ("Skylake")
MPI: No. of CPUs	1	48
CPU Time	2 h 35 mins	1 h 02 mins
Time Step Size	$5 \times 10^{-4} s$	$5 \times 10^{-4} s$
Simulation Time	5 s	5 s

The velocity and vorticity comparison at location A, B, C, and D (demonstrated in Figure 4.13) are shown from Figure 4.18 to Figure 4.28 below:

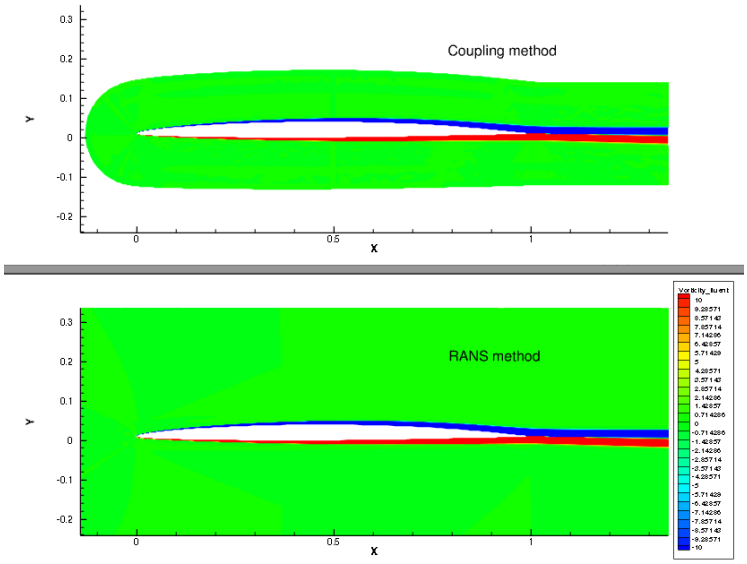

Figure 4.18: Vorticity contour at t =5 s, turbulent flow, Re=2×10^6 , hydrofoil case.

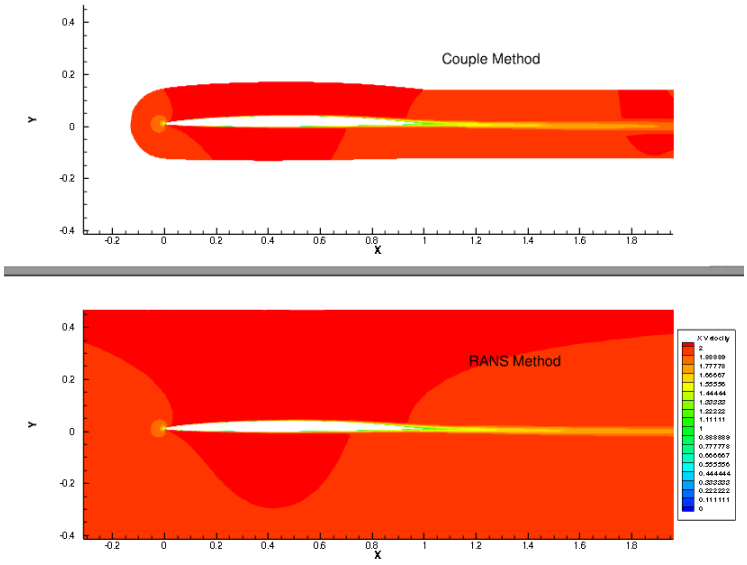

Figure 4.19: X-Velocity contour comparison at t =5 s, turbulent flow, Re=2×10^6 , hydrofoil case.

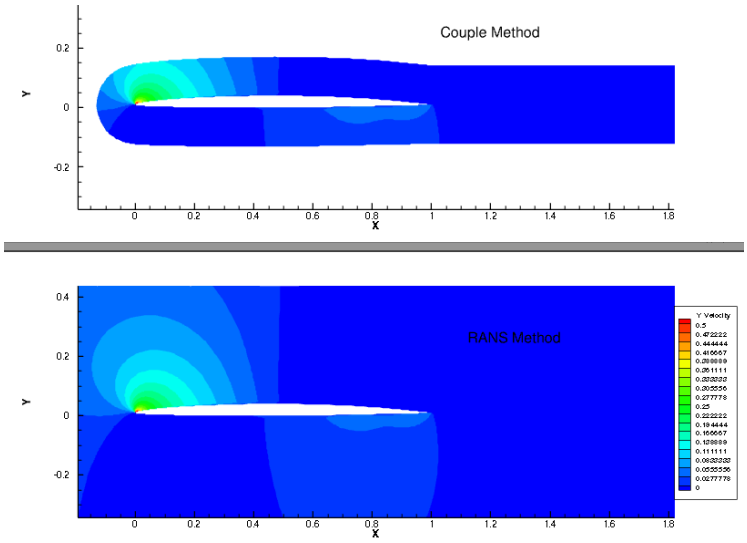

Figure 4.20: Y-Velocity contour comparison at t =5 s, turbulent flow, Re=2×10^6 , hydrofoil case.

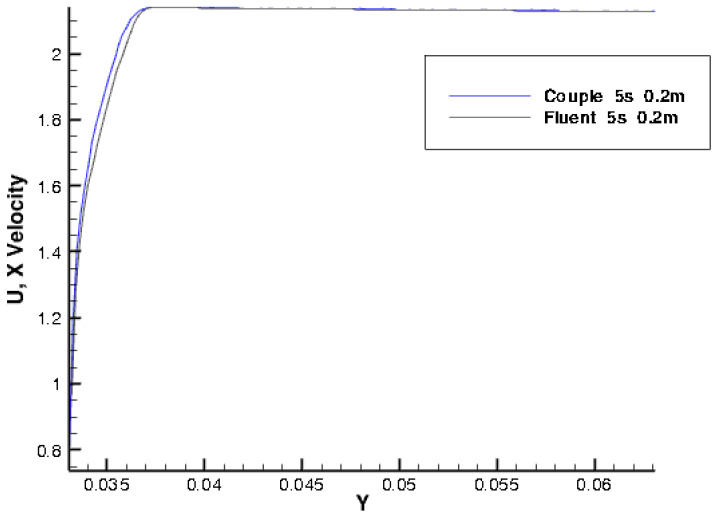

Figure 4.21: X-Velocity profile at A at t =5 s, turbulent flow, Re=2×10^6, hydrofoil case.

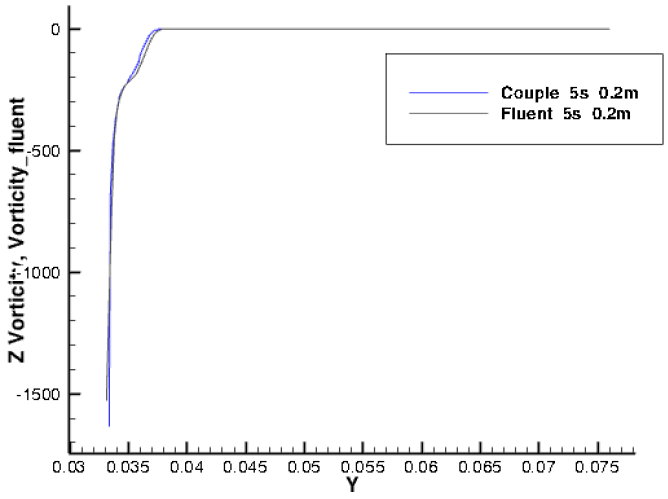

Figure 4.22: Vorticity profile at A at t =5 s, turbulent flow, Re=2×10^6, hydrofoil case.

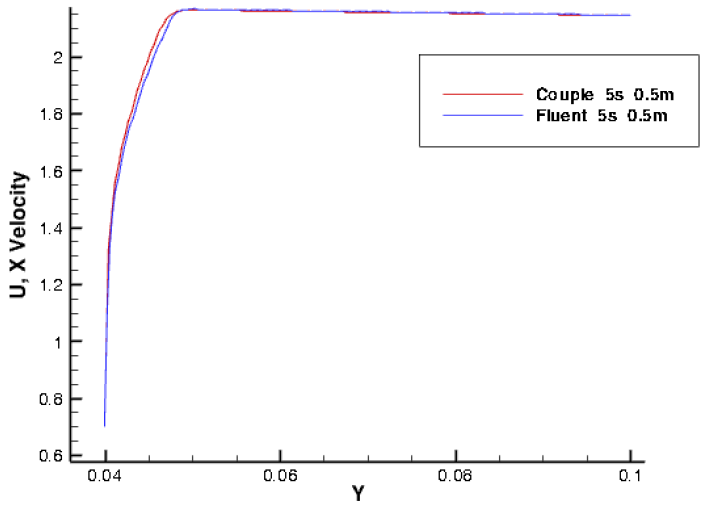

Figure 4.23: X-Velocity profile at B at t =5 s, turbulent flow, Re=2×10^6, hydrofoil case.

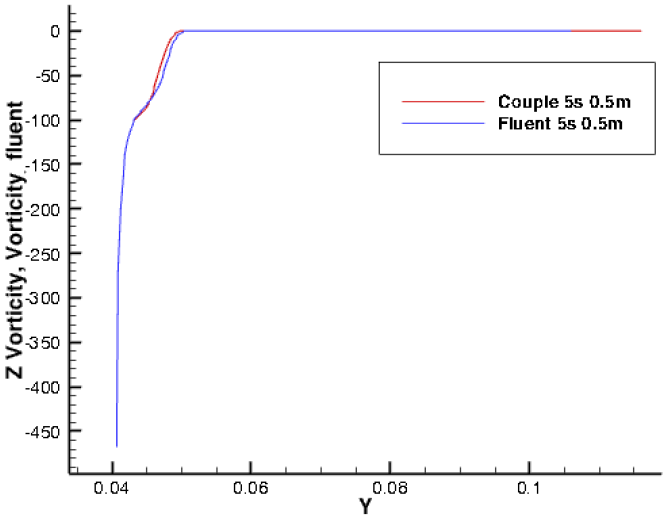

Figure 4.24: Vorticity profile at B at t =5 s, turbulent flow, Re=2×10^6, hydrofoil case.

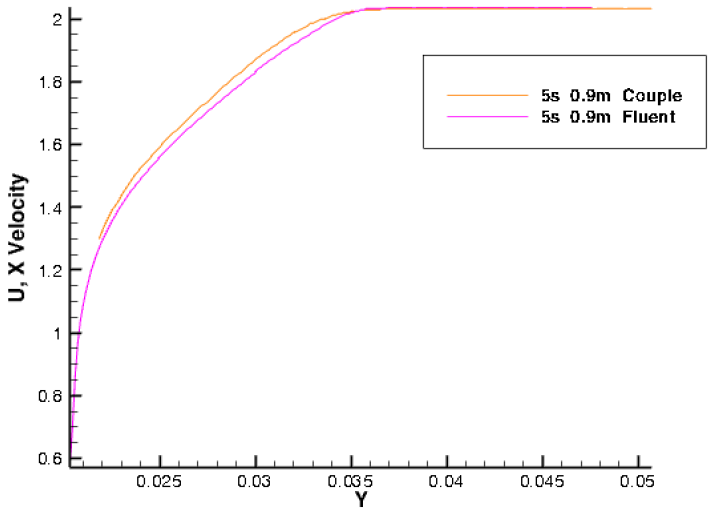

Figure 4.25: X-Velocity profile at C at t =5 s, turbulent flow, Re=2×10^6, hydrofoil case.

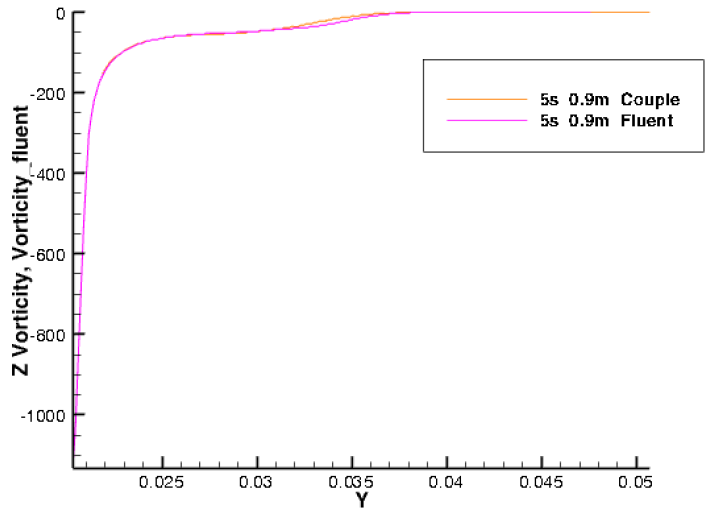

Figure 4.26: Vorticity profile at C at t =5 s, turbulent flow, Re=2×10^6, hydrofoil case.

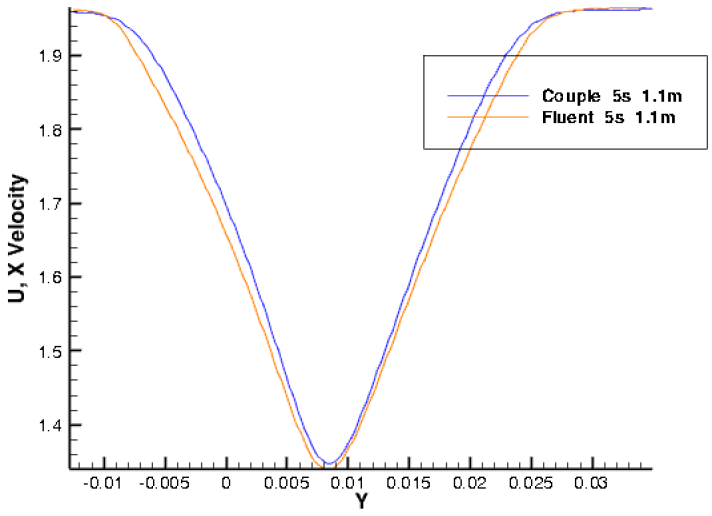

Figure 4.27: X-Velocity profile at D at t =5 s, turbulent flow, Re=2×10^6, hydrofoil case.

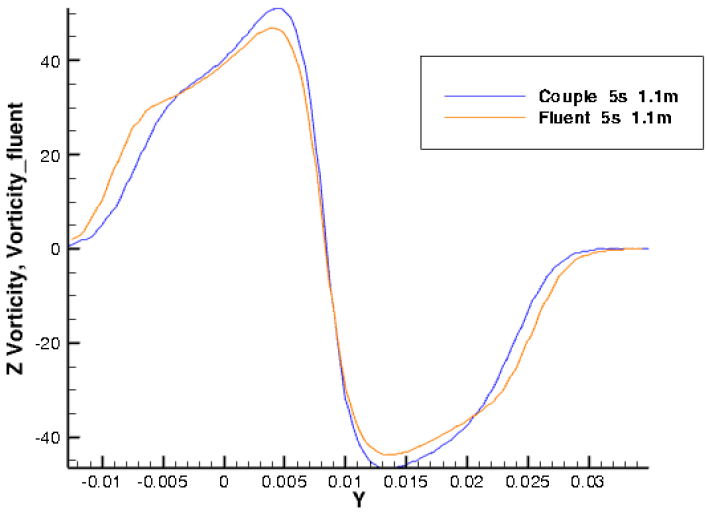

Figure 4.28: Vorticity profile at D at t =5 s, turbulent flow, Re=2×10^6, hydrofoil case.

The pressure coefficients comparison between the coupling method and the RANS method (implemented by OpenFOAM) are shown in Figure 4.29.

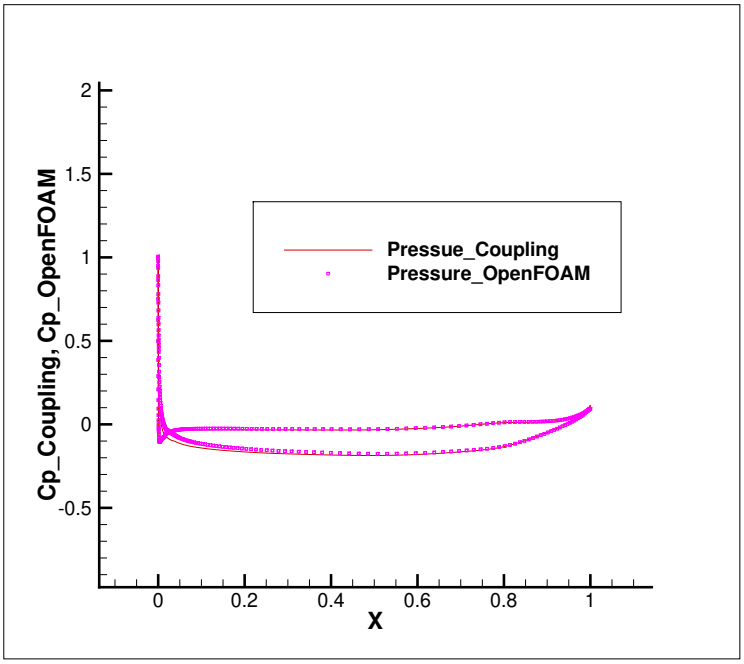

Figure 4.29: Pressure coefficients comparison at t =5 s, turbulent flow, Re=2×10^6, hydrofoil case.

The velocity profile and the vorticity profile of the coupling method agree well with the FLUENT results at the leading edge and the trailing edge. However, the deviation between them will become appreciable in the wake area (x= 1.1m). This is because in equation (3.17) the three additional terms $2\frac{\partial^2(\nu_m+\nu_\tau)}{\partial z^2}\frac{\partial \omega}{\partial x}$, $-2\frac{\partial^2(\nu_m+\nu_\tau)}{\partial x^2}\frac{\partial u}{\partial z}$, and $4\frac{\partial^2(\nu_m+\nu_\tau)}{\partial x \partial z}\frac{\partial u}{\partial x}$, which exist on the RHS of turbulent vorticity equation (3.15), have been ignored.

4.2.1.3 Re = 10^6

The velocity of the incoming flow is 1 m/s with the angle of attack to be 0 degree. The Reynolds number in the viscous case was specified to be 10^6.

The pressure coefficients comparison between the coupling method and the RANS method (implemented by OpenFOAM) are shown in Figure 4.30.

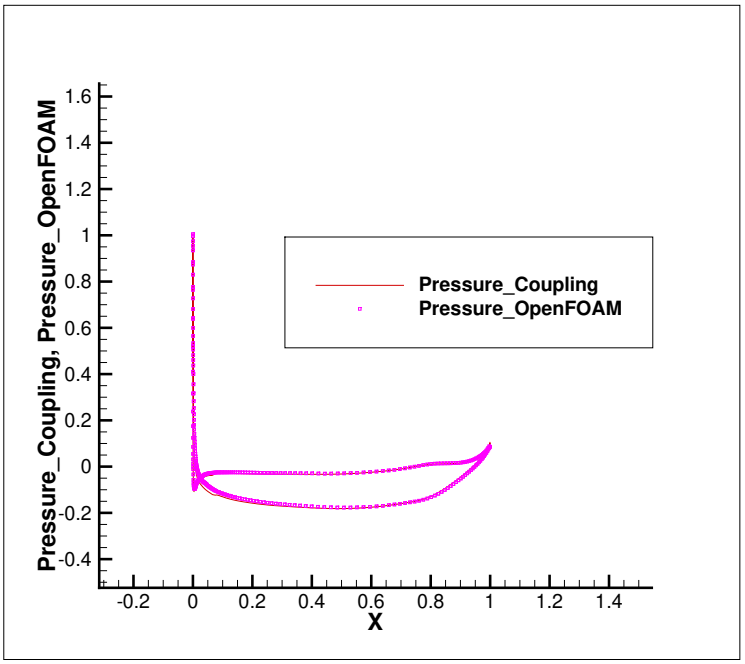

Figure 4.30: Pressure coefficients comparison at t =5 s, turbulent flow, Re=10^6, hydrofoil case.

4.2.1.4 Re = 4×10^6

The velocity of the incoming flow is 4 m/s with the angle of attack to be 0 degree. The Reynolds number in the viscous case was specified to be 4×10^6.

The pressure coefficients comparison between the coupling method and the RANS method (implemented by OpenFOAM) are shown in Figure 4.31.

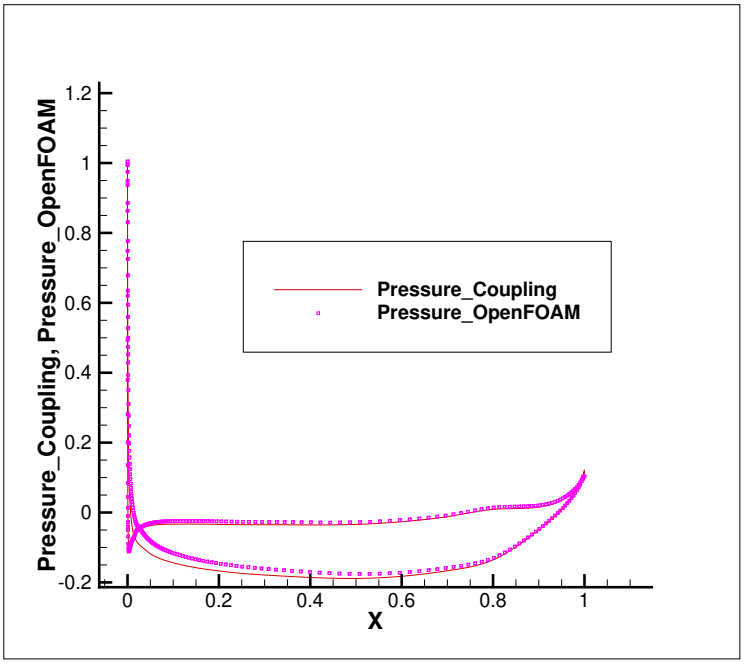

Figure 4.31: Pressure coefficients comparison at t =5 s, turbulent flow, Re=4×10^6, hydrofoil case.

4.2.1.5 Convergence Study

In order to validate the grid independence of the coupling method, different sizes and different number of elements on the direction normal to the hydrofoil surface have been applied to the coupling method to predict the flow around the hydrofoil in turbulent case. Three cases are designed as shown in Table 4.8. The tests are run at $Re = 2 \times 10^6$, $AOA = 0^o$. The vorticity, x-velocity, and y-velocity at the half chord length from different cases agrees

very well with each other as shown from Figure 4.32 to Figure 4.34, which validates the convergence of the coupling method in the hydrofoil turbulent case.

Table 4.8: Cases setting for grid independence study in turbulent foil cases, $Re = 2 \times 10^6$.

Case No.	No. of Layers of Cell	First Layer Height/ m	Expansion Ratio in Block 1	No. of Elements on the Wake	Expansion Ratio in Block 2
1	50	1×10^{-4}	1.05	85	1.095
2	60	1×10^{-4}	1.05	95	1.095
3	70	1×10^{-4}	1.05	105	1.095

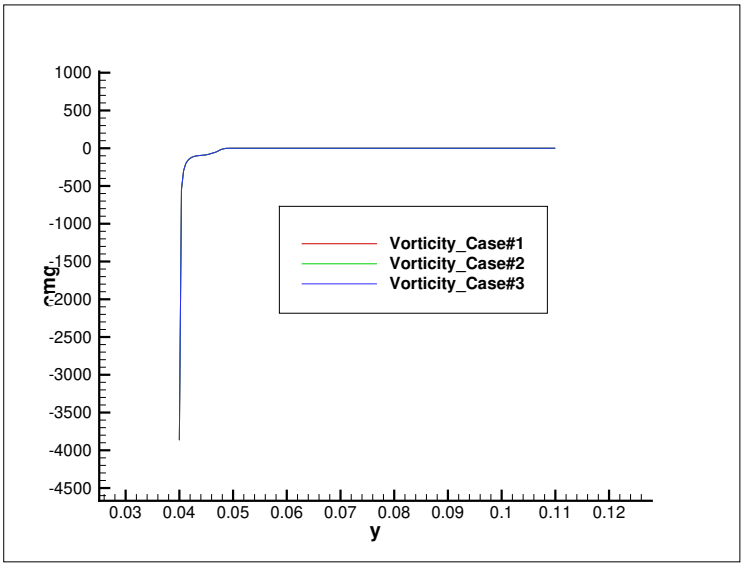

Figure 4.32: Comparison of vorticity at 50% chord length for different cases, $Re = 2 \times 10^6$, hydrofoil case.

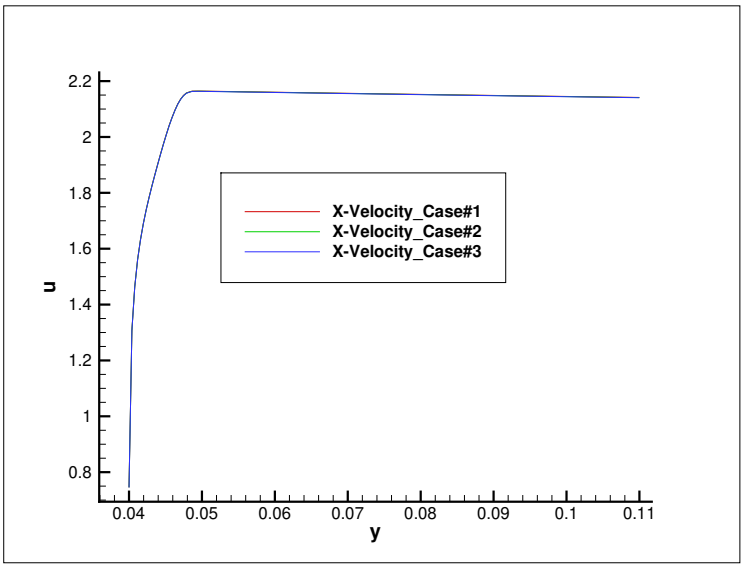

Figure 4.33: Comparison of X-velocity at 50% chord length for different cases, $Re = 2 \times 10^6$, hydrofoil case.

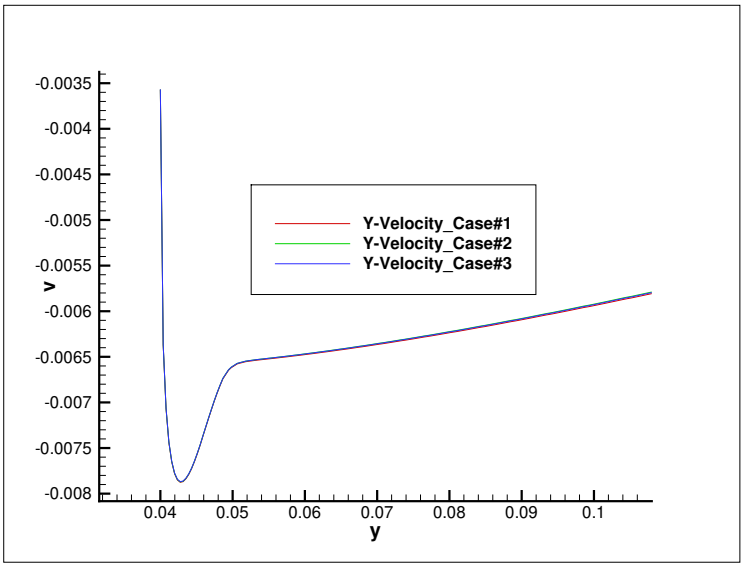

Figure 4.34: Comparison of Y-velocity at 50% chord length for different cases, $Re = 2 \times 10^6$, hydrofoil case.

4.2.2 Turbulent Flow around a Cylinder Case

The coupling method is also applied in the case of the 2-D cylinder. The diameter of the cylinder is 1 meter. The velocity of the incoming flow is 1 m/s. The Reynolds number in the cylinder case was specified to be 10^6 . The comparison is made between the coupling method and the RANS method.

4.2.2.1 Grid Configuration

RANS: As shown in the convergence study in the next sub-section, the domain parameters of Case #3 are good enough for the calculation to converge. Thus, we set the domain parameters to be the same as the ones in Case #3. Domain for RANS method is described in Table 4.9 and Figure 4.35.

Table 4.9: Domain parameters of RANS method for turbulent cylinder case, Re = 10^6.

Cell Number	No. of Layers of Cell	First Layer Height/ m	Expansion Ratio	Time Step Size/ s
323,000	300	0.0002	1.05	0.001

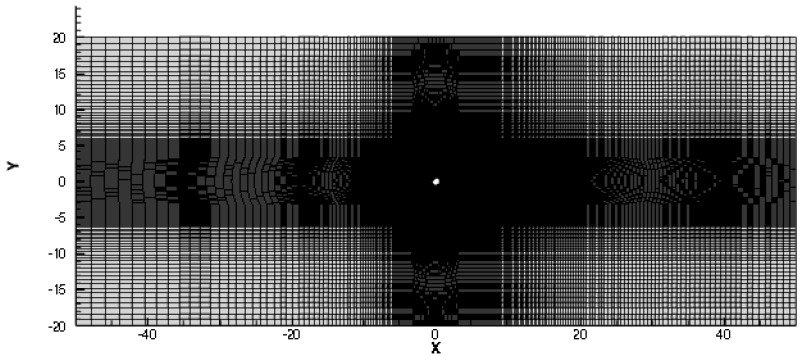

Figure 4.35: Grids for RANS domain for turbulent cylinder case, Re=10^6 .

The coupling method: Domain for coupling method is described in Table 4.10 and Figure 4.36.

Table 4.10: Domain parameters for the coupling method for turbulent cylinder case, Re = 10^6.

Cell Number	Elements on the Cylinder	No. of Layer of Cells	First Layer Height/ m	Expansion Ratio	Time Step Size/ s
35,400	300	118	0.001	1.05	0.001

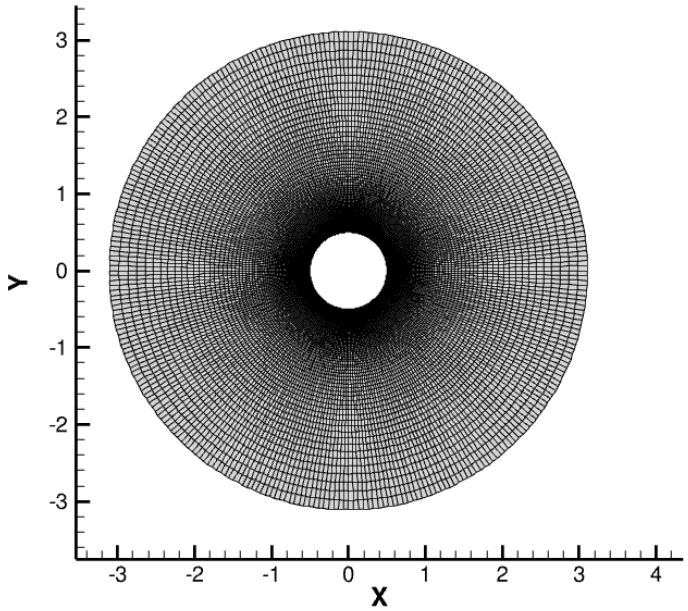

Figure 4.36: Grids for coupling method domain for turbulent cylinder case, Re=10^6 .

4.2.2.2 Comparison between two Methods

The simulation time and CPU cost comparison is shown in Table 4.11.

Table 4.11: Simulation time and CPU cost comparison for turbulent cylinder case, Re=10^6.

	Coupling Method	Fluent
Node Type	Intel Xeon Platinum 8160 ("Skylake")	Intel Xeon Platinum 8160 ("Skylake")
MPI: No. of CPUs	1	48
CPU Time	6 h 59 mins	9 h 02 mins
Time Step Size	$5 \times 10^{-4} s$	$5 \times 10^{-4} s$
Simulation Time	29 s	50 s

The CPU time of the coupling method and the RANS method are comparable. Since coupling method uses only 1 CPU and RANS method uses 48, the calculation speed of the coupling method has huge potential for improvement and can definitely be superior in speed than RANS method if parallel computing is achieved.

The vorticity and velocity comparisons are shown from Figure 4.38 to Figure 4.49. Location A and location B are shown in Figure 4.37:

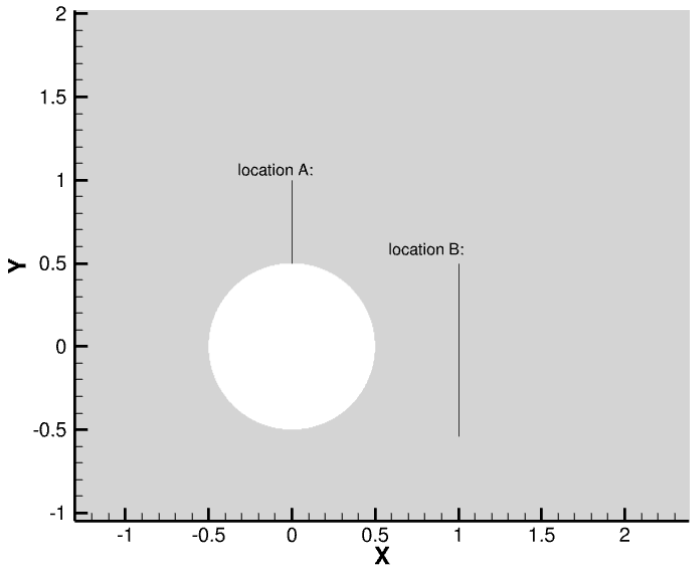

Figure 4.37: Demonstration for location A and B, Re=10^6.

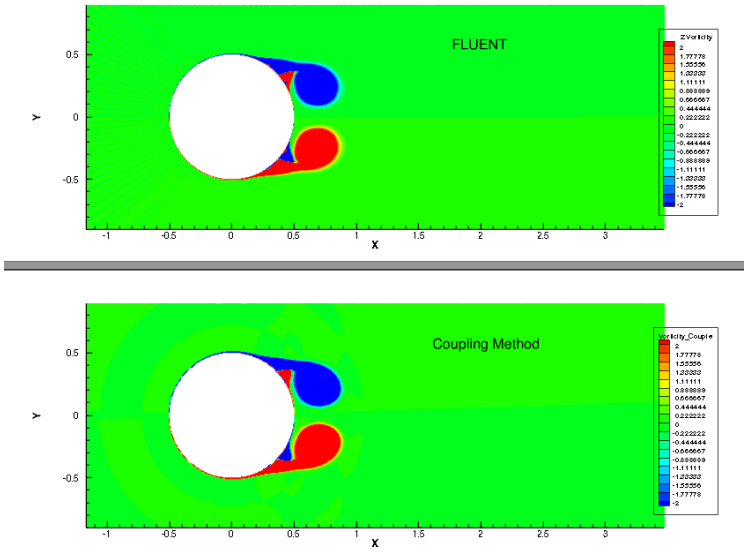

Figure 4.38: Vorticity contour at t =2s, turbulent flow, Re=10^6, cylinder case.

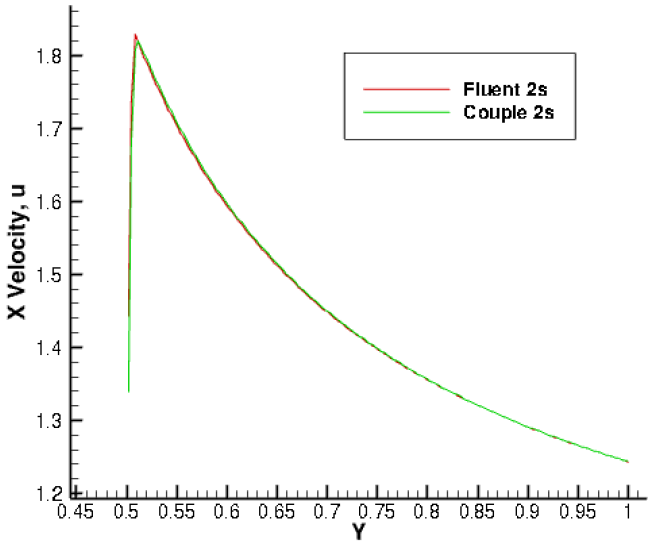

Figure 4.39: X-Velocity profile at location A at t =2s, turbulent flow, Re=10^6, cylinder case.

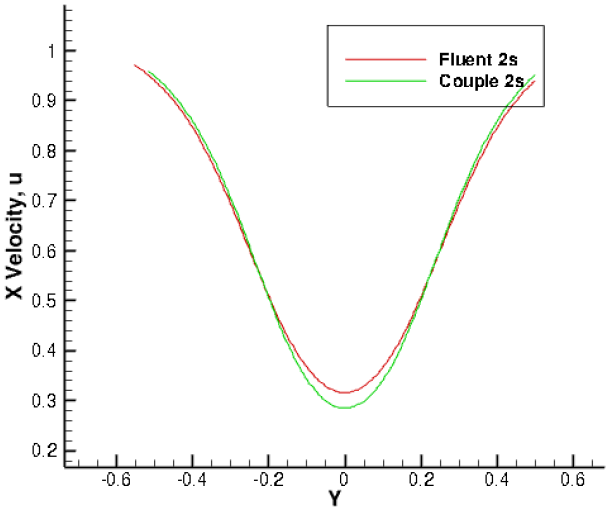

Figure 4.40: X-Velocity profile at location B at t =2s, turbulent flow, Re=10^6, cylinder case.

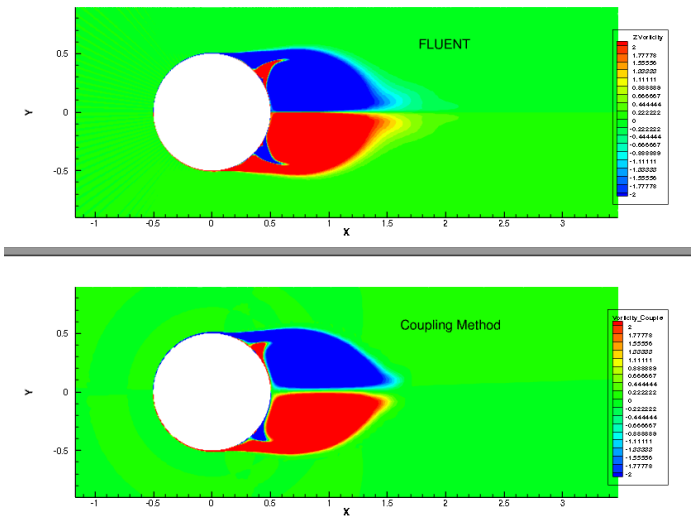

Figure 4.41: Vorticity contour at t =4s, turbulent flow, Re=10^6, cylinder case.

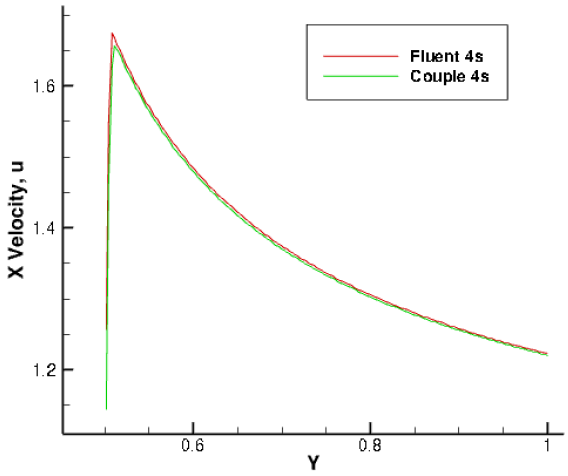

Figure 4.42: X-Velocity profile at location A at t =4s, turbulent flow, Re=10^6, cylinder case.

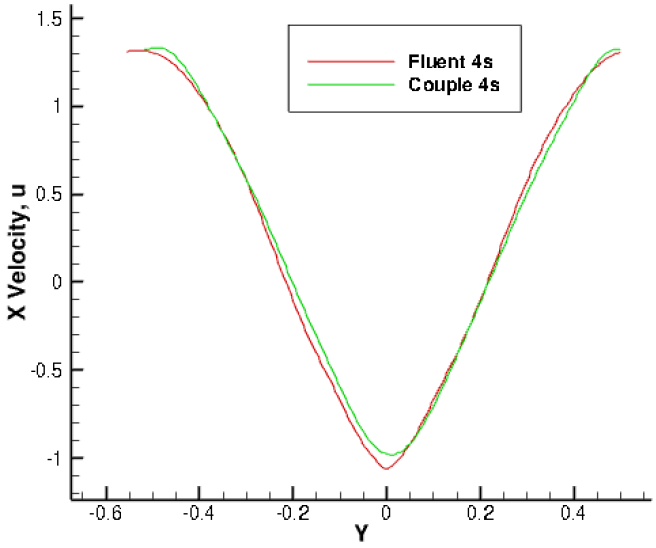

Figure 4.43: X-Velocity profile at location B at t =4s, turbulent flow, Re=10^6, cylinder case.

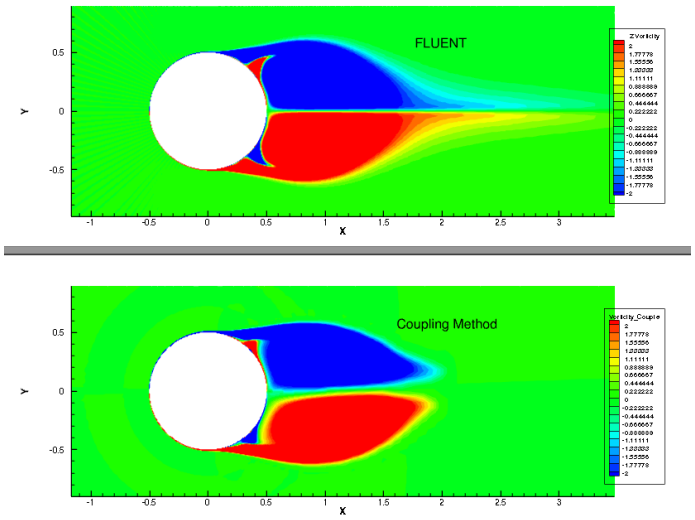

Figure 4.44: Vorticity contour at t =6s, turbulent flow, Re=10^6, cylinder case.

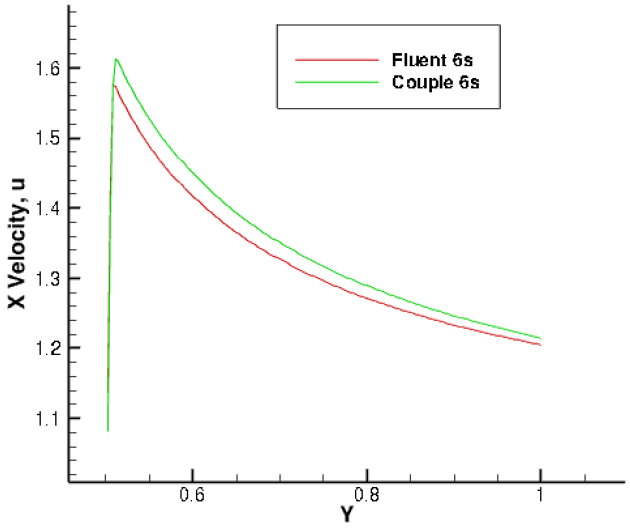

Figure 4.45: X-Velocity profile at location A at t =6s, turbulent flow, Re=10^6, cylinder case.

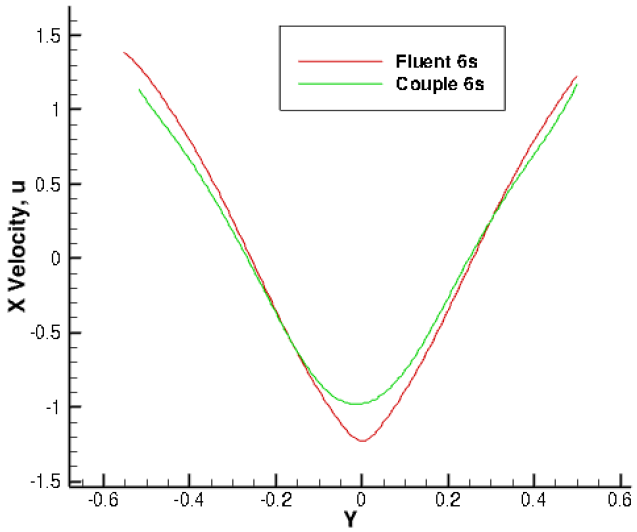

Figure 4.46: X-Velocity profile at location B at t =6s, turbulent flow, Re=10^6, cylinder case.

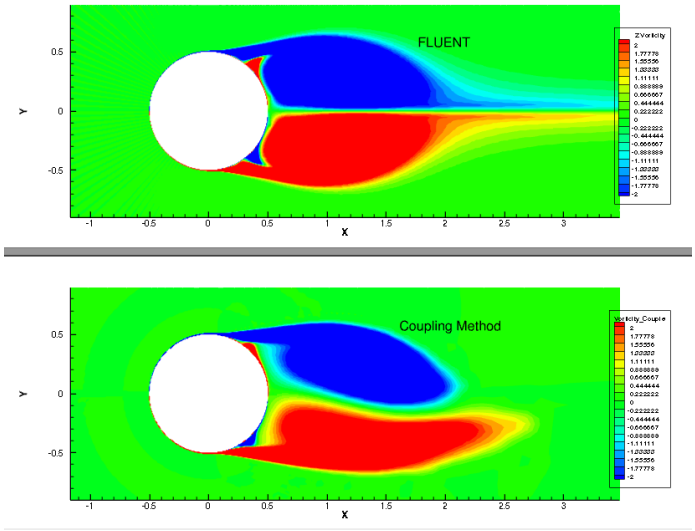

Figure 4.47: Vorticity contour at t =8s, turbulent flow, Re=10^6, cylinder case.

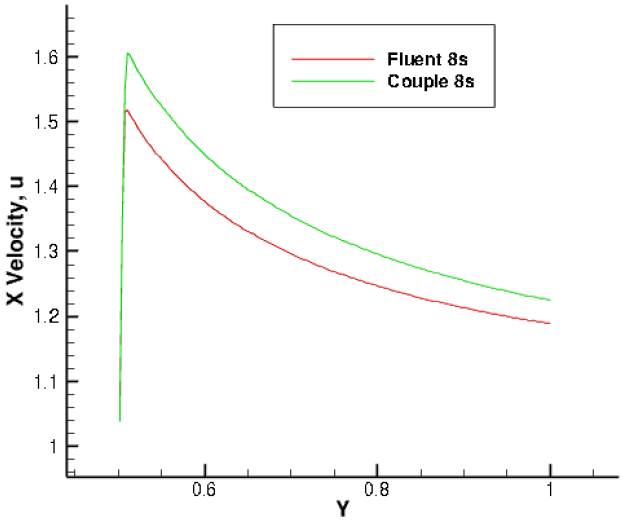

Figure 4.48: X-Velocity profile at location A at t =8s, turbulent flow, Re=10^6, cylinder case.

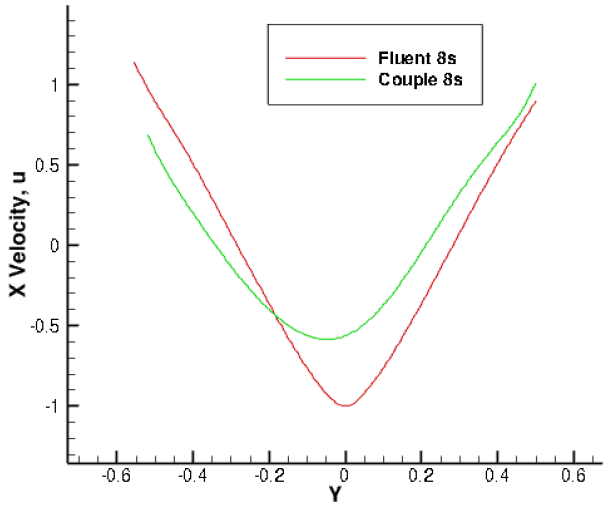

Figure 4.49: X-Velocity profile at location B at t =8s, turbulent flow, Re=10^6, cylinder case.

The velocity profile and vorticity contour of the coupling method agree well with the Fluent results at the initial stage. However, the deviation keeps increasing as time increases. This discrepancy might be due to the fact that the hydrofoil assumption $\frac{\partial}{\partial z} \gg \frac{\partial}{\partial x}$ is not valid to the cylinder case, and the three additional terms $2\frac{\partial^2(\nu_m+\nu_\tau)}{\partial z^2}\frac{\partial \omega}{\partial x}$, $-2\frac{\partial^2(\nu_m+\nu_\tau)}{\partial x^2}\frac{\partial u}{\partial z}$, and $4\frac{\partial^2(\nu_m+\nu_\tau)}{\partial x \partial z}\frac{\partial u}{\partial x}$ cannot be ignored.

4.2.2.3 Convergence Study

The grid independence study is made for the RANS run. Three RANS simulations with different domain parameters are conducted and the results are compared. Table 4.12 shows the domain parameters for these three grids.

Table 4.12: Convergence study: parameters of 3 RANS domain for turbulent cylinder case, Re = 10^6.

Case No.	Elements on Cylinder	Number of the Layer of Cells	First Layer Height/ m	Elements in Forwarding Direction	Elements in Backward Direction	Total Cell Number
1	800	600	2×10^{-4}	150	400	740,000
2	800	400	2×10^{-4}	100	270	473,800
3	800	300	2×10^{-4}	75	135	323,000

The Drag coefficients comparison is in Figure 4.50. The 3 results agree well with each other, which means the 3 grids are all good enough. Thus, Case #3 has the best grids for the RANS simulation since it can provide both computational efficiency and accuracy.

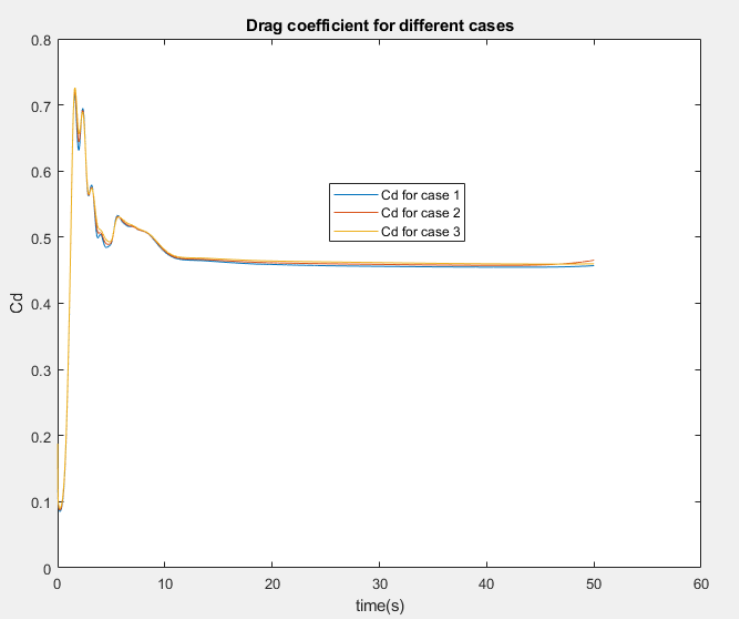

Figure 4.50: Drag coefficients comparison for three RANS simulations, turbulent flow, Re=10^6.

Chapter 5

Results and Discussions

5.1 Turbulent Flow around a 2-D Hydrofoil Case

For the case of turbulent flow around a hydrofoil[1], the pressure coefficients of the coupling method agrees well with the RANS result at different Reynolds numbers.

The velocity profile of the coupling method agrees well with the Fluent result[2] at the leading edge (x=0.2m). However, the deviation between them will become larger as x increases. For instance, the deviation shown in the Figure 4.27 (x=1.1m) is larger than the one in the Figure 4.21 (x=0.2m). This might be because in equation (3.17) the three additional terms $2\frac{\partial^2(\nu_m+\nu_\tau)}{\partial z^2}\frac{\partial \omega}{\partial x}$, $-2\frac{\partial^2(\nu_m+\nu_\tau)}{\partial x^2}\frac{\partial u}{\partial z}$, and $4\frac{\partial^2(\nu_m+\nu_\tau)}{\partial x \partial z}\frac{\partial u}{\partial x}$ which exist on the RHS of turbulent vorticity equation (3.15), have been ignored[3].

At the leading edge, the turbulent viscosity is smaller and these ignored terms are expected to be smaller. However, as the flow goes around

[1]The main work of this thesis is based on Yao and Kinnas [17]. Even though the formulation of the turbulent vorticity equation was derived by Dr. Kinnas, the coupling of the VISVE method with OpenFOAM was implemented and tested by the author of this thesis.

[2]The Fluent results were achieved with sufficient grid resolution so that they were grid independent.

[3]The results from the current method were shown to be grid independent.

the hydrofoil from leading edge to trailing edge and the turbulent viscosity increases, these ignored terms $2\frac{\partial^2(\nu_m+\nu_\tau)}{\partial z^2}\frac{\partial \omega}{\partial x}$, $-2\frac{\partial^2(\nu_m+\nu_\tau)}{\partial x^2}\frac{\partial u}{\partial z}$, and $4\frac{\partial^2(\nu_m+\nu_\tau)}{\partial x \partial z}\frac{\partial u}{\partial x}$ will become larger. Thus, the deviation between the coupling method and Fluent will accumulate and finally become an appreciable value as the flow goes from the leading edge to the wake area.

5.2 Turbulent Flow around a 2-D Cylinder Case

For the case of turbulent flow around a cylinder, the velocity profiles and vorticity contours of the coupling method agree well with the Fluent results at the initial stage.

However, the deviation keeps increasing as time increases. To be more specific, the coupling method predicts vortex induced vibration (VIV) at 4 seconds while the Fluent method does not predict VIV until long after. This discrepancy might be due to the fact that the hydrofoil assumption is not valid to the cylinder case, partly the three additional terms cannot be ignored.

Chapter 6

Conclusions and Future Work

6.1 Conclusions

A synchronous coupling method has been implemented to solve the turbulent flow around 2-D hydrofoils and 2-D cylinders [1]. The results agree well with RANS method in 2-D hydrofoil case but deviate in cylinder case as time increases. This may due to the fact that the hydrofoil assumption is no longer applicable to cylinder case and the 3 additional terms $2\frac{\partial^2(\nu_m+\nu_\tau)}{\partial z^2}\frac{\partial \omega}{\partial x}$, $-2\frac{\partial^2(\nu_m+\nu_\tau)}{\partial x^2}\frac{\partial u}{\partial z}$, and $4\frac{\partial^2(\nu_m+\nu_\tau)}{\partial x \partial z}\frac{\partial u}{\partial x}$ cannot be ignored in the turbulent vorticity equation.

6.2 Future Work

More needs to be done in the future along the following directions

- The 3 additional terms will be included in the turbulent vorticity equation.
- The pressures and forces evaluation methods will be improved in the

[1] The main work of this thesis is based on Yao and Kinnas [17]. Even though the formulation of the turbulent vorticity equation was derived by Dr. Kinnas, the coupling of the VISVE method with OpenFOAM was implemented and tested by the author of this thesis.

turbulent cases, and these improved evaluation methods will be applied in both 2-D hydrofoil and 2-D cylinder cases. In particular, the effect of the turbulent viscosity ν_τ will be included in the calculation of pressures. The pressures and forces will be calculated by the improved evaluation methods and compared with those obtained from other methods and experiments.

- Finally, this coupling method will be extended in the case of turbulent flow around 3-D hydrofoils and propellers.

Bibliography

[1] ANSYS-fluent. `https://www.ansys.com/products/fluids/ansys-fluent`. Accessed January 14th, 2019.

[2] G. K. Batchelor. *An Introduction to Fluid Dynamics*. Cambridge University Press, 1967.

[3] J. P. Giesing. Nonlinear two-dimensional unsteady potential flow with lift. *Journal of Aircraft*, 5(2):135–143, 1968.

[4] J. Katz. A discrete vortex method for the non-steady separated flow over an airfoil. *Journal of Fluid Mechanics*, 102:315–328, 1981.

[5] S. A. Kinnas. Vorticity equation for turbulent flows with variable density and viscosity. *(under preparation)*, 2019.

[6] S. A. Kinnas and C. Y. Hsin. The local error of a low-order boundary element method at the trailing edge of a hydrofoil and its effect on the global solution. *Computers and fluids*, 23(1):63–75, 1994.

[7] Z. Li and S.A. Kinnas. Visve, a vorticity based model applied to unidirectional and alternating flow around a cylinder. In *22nd SNAME Offshore Symposium, Houston, Texas, USA, February*, 2017.

[8] S. B. Pope. *Turbulent flows*. Cambridge University Press, 2000.

[9] Y. Tian. *Leading edge vortex modeling and its effect on propulsor performance*. PhD thesis, Ocean Engineering Group, The University of Texas at Austin, 2014.

[10] Y. Tian and S. A. Kinnas. A viscous vorticity method for propeller tip flows and leading edge vortex. In *4th Symposium on Marine Propulsors, SMP. Vol. 15.*, 2015.

[11] C. H. Williamson. Vortex dynamics in the cylinder wake. *Annual review of fluid mechanics*, 28(1):477–539, 1996.

[12] C. Wu and S.A. Kinnas. A distributed vorticity model for flow past a 3-d hydrofoil. In *24th SNAME Offshore Symposium, Texas, Houston, February 20th*, 2019.

[13] C. Wu, L. Xing, and S.A. Kinnas. A viscous vorticity equation (visve) method applied to 2-d and 3-d hydrofoils in both forward and backing conditions. In *23rd SNAME Offshore Symposium, Texas, Houston, February 14th*, 2018.

[14] Y. Wu. A vorticity based model and its application to flow around an impulsively started cylinder. Master's thesis, Ocean Engineering Group, The University of Texas at Austin, 2016.

[15] L. Xing. Visve, a vorticity based model applied to 2-d hydrofoils in backing and cavitating conditions. Master's thesis, Ocean Engineering Group, The University of Texas at Austin, 2018.

[16] L. Xing, C. Wu, and S.A. Kinnas. Visve, a vorticity based model applied to cavitating flow around a 2-d hydrofoil. In *Proceedings of the 10th International Symposium on Cavitation (CAV2018). ASME Press.*, 2018.

[17] H. Yao and S.A. Kinnas. Coupling viscous vorticity equation (visve) method with openfoam to predict turbulent flow around 2-d hydrofoils and cylinders (accepted). In *29th ISOPE Conference, Honolulu, Hawaii, USA, June*, 2019.